1

Boron isotopic composition of olivine-hosted melt inclusions from Gorgona komatiites,

Colombia: new evidence supporting wet komatiite origin

Andrey A. Gurenko[1,2]*, Vadim S. Kamenetsky[3]

[1] Woods Hole Oceanographic Institution, Geology & Geophysics, Woods Hole, MA 02543,
USA

[2] Centre de Recherches Pétrographiques et Géochimiques, CNRS-Nancy Université, BP 20, F-
54501 Vandoeuvre-lès-Nancy, France

[3] School of Earth Sciences and Centre for Ore Deposit Research, University of Tasmania,
Australia

Revised version submitted to

Earth and Planetary Science Letters

Components:

Abstract: 316 words; 2,064 characters with spaces;

Main text: 6,473 words; 40,573 characters with spaces;

5 figures, 2 tables;

List of references includes 91 citations.

On-line supplementary Material: Analytical Methods, 2 figures

* Corresponding author and present address:

Andrey A. Gurenko, Centre de Recherches Pétrographiques et Géochimiques, 15, rue Notre-Dame des Pauvres, B.P.

20, 54501 Vandoeuvre-lès-Nancy, France. Phone: +33 (0)3 83 59 48 75, Fax: +33 (0)3 83 51 17 98, E-mail:

agurenko@crpg.cnrs-nancy.fr

30 **Abstract –** A fundamental question in the genesis of komatiites is whether these rocks originate

31 from partial melting of dry and hot mantle, 400–500°C hotter than typical sources of MORB and

32 OIB magmas, or if they were produced by hydrous melting of the source at much lower

33 temperatures, similar or only moderately higher than those known today. Gorgona Island,

34 Colombia, is a unique place where Phanerozoic komatiites occur and whose origin is directly

35 connected to the formation of the Caribbean Large Igneous Province. The genesis of Gorgona

36 komatiites remains controversial, mostly because of the uncertain origin of volatile components

37 which they appear to contain. These volatiles could equally result from shallow level magma

38 contamination, melting of a "damp" mantle or fluid-induced partial melting of the source due to

39 devolatilization of the ancient subducting plate. We have analyzed boron isotopes of olivine-

40 hosted melt inclusions from the Gorgona komatiites. These inclusions are characterized by

41 relatively high contents of volatile components and boron (0.2–1.0 wt.% H_2O, 0.05–0.08 wt.%

42 S, 0.02–0.03 wt.% Cl, 0.6–2.0 µg/g B), displaying positive anomalies in the overall depleted,

43 primitive mantle (PM) normalized trace element and REE spectra ($[La/Sm]_n$ = 0.16–0.35;

44 $[H_2O/Nb]_n$ = 8–44; $[Cl/Nb]_n$ = 27–68; $[B/Nb]_n$ = 9-30, assuming 300 µg/g H_2O, 8 µg/g Cl and

45 0.1 µg/g B in PM; Kamenetsky et al., 2010. Composition and temperature of komatiite melts

46 from Gorgona Island constrained from olivine-hosted melt inclusions. Geology 38, 1003–1006).

47 The inclusions range in $\delta^{11}B$ values from −11.5 to +15.6 ± 2.2‰ (1 SE), forming two distinct

48 trends in a $\delta^{11}B$ vs. B-concentration diagram. Direct assimilation of seawater, seawater-derived

49 components, altered oceanic crust or marine sediments by ascending komatiite magma cannot

50 readily account for the volatile contents and B isotope variations. Alternatively, injection of <3%

51 of a ^{11}B enriched fluid to the mantle source could be a plausible explanation for the $\delta^{11}B$ range

52 that also may explain the H_2O, Cl and B excess.

53

54 **Keywords** Komatiites, Gorgona Island, Melt inclusions, Volatile components, Boron isotopes,

55 Ion microprobe

56

57

1. Introduction

The Island of Gorgona, Colombia, is a unique place where Phanerozoic komatiites have been first described and then studied in detail (Gansser, 1950; Echeverría, 1980; Aitken and Echeverría, 1984; Echeverría and Aitken, 1986; Kerr et al., 1996; Kerr, 2005; Sinton et al., 1998; Walker et al., 1991, 1999; Révillon et al., 2000, 2002; Serrano et al., 2011). The problem of the origin of Gorgona komatiites is directly connected to the origin of the Caribbean oceanic plateau (also called the Caribbean Large Igneous Province or CLIP; see review by Hastie and Kerr, 2010). The plateau is the remnant of one or more oceanic melting anomalies active during the late Cretaceous in the Pacific realm and represents a large outpouring of mafic volcanism. The main question is whether the mafic volcanic rocks of the Caribbean plateau were erupted onto the Farallon plate and then subsequently transported during the late Cretaceous to the northeast, having collided with a large intra-oceanic arc (i.e., the Great Arc of the Caribbean) or whether formation of the CLIP was related to the opening a large slab window produced by the intersection of the proto-Caribbean spreading ridge with the Great Caribbean Arc (Pindell et al., 2006; Pindell and Kennan, 2009; Hastie and Kerr, 2010 and references therein). Previous age determinations of the Gorgona mafic rocks yielded ages ranging from ~86 to ~92 Ma (Aitken and Echeverría, 1984; Sinton et al., 1998; Walker et al., 1999), more consistent with the first hypothesis where the Galapagos plume head impacted the Farallon plate. However, a recent set of robust ^{40}Ar-^{39}Ar ages (Serrano et al., 2011) obtained for the main types of Gorgona mafic rocks (komatiites, peridotites, gabbros, picritic basalts) documents much longer magmatic activity on the island, spanning from ~99 to ~61 Ma. This data questions, in fact, the broadly accepted model suggesting that the Caribbean Large Igneous Province formed ultimately due to melting of a plume head at ~90 Ma. Furthermore, Serrano et al. (2011) have demonstrated that multiple magmatic pulses over several tens of Ma, which resulted in a long period of diffuse magmatism without a clear pattern of migration recognized as within a small area like Gorgona Island as in other Caribbean LIP areas, can be broadly coeval with the opening of the Caribbean slab window between ~100 and ~66 Ma.

The abundances of volatile components in komatiitic magmas represent a central issue in their origin because the presence of volatiles in the mantle source considerably affect peridotite

87   solidus, shifting it to lower temperature and pressure and thus this information is essential to

88   constrain the thermal and chemical evolution of the deep Earth. The controversy remains as to

89   whether komatiites represent the products of essentially dry and hot melting of the mantle or

90   whether they result from melting of rising wet plumes, which gained their volatiles by slab

91   dehydration during subduction (e.g., Allègre, 1982; Arndt et al., 1997; 1998; Parman et al., 1997;

92   Litasov and Ohtani, 2002; Wilson et al., 2003; Grove and Parman, 2004; Herzberg, 1995;

93   Herzberg et al., 2007; Berry et al., 2008 among others). Although many existing studies are

94   traditionally skeptical about a wet origin of the Archaean komatiites (e.g., Arndt et al., 1998 and

95   references therein), numerous petrological, geochemical and experimental data indicate, for

96   instance, that komatiites from the 3.5 Ga Barberton Greenstone Belt and from 3.3 Ga

97   Commondale, South Africa are hydrous, characterized by somewhat elevated SiO_2 contents,

98   exhibit boninite-like trace element spectra and are believed to have formed due to subduction

99   zone impact (e.g., Wilson et al., 2003; Grove and Parman, 2004). In addition, several recent

100   studies utilizing the melt inclusion approach and focusing on the 2.7-Ga-old Belingwe

101   komatiites, Zimbabwe, have argued that primary komatiitic magmas may contain up to 1 wt.%

102   H_2O, but the source of water appears to be controversial (shallow depth magma contamination

103   versus melting of a hydrous mantle plume source; Shimizu et al., 2001; Berry et al., 2008; Kent

104   et al., 2009).

105   Although melt inclusions in minerals are routinely used to assess temperature, pressure

106   and redox conditions of magma crystallization, chemical composition and the volatile budget of

107   many rock types (e.g., Sobolev and Danyshevsky, 1994; Sobolev and Chaussidon, 1996;

108   Gurenko and Chaussidon, 1995, 1997; Kent et al., 1999; Danyushevsky et al., 2002a; Rose et al.,

109   2001; Gurenko et al., 2005; Le Voyer et al., 2008), the melt inclusion approach has not been

110   widely used to investigate komatiites, apart from a few studies (McDonough and Ireland, 1993;

111   Shimizu et al., 2001; 2009; Danyshevsky et al., 2002b; Berry et al., 2008; Kent et al., 2009;

112   Kamenetsky et al., 2010). In part, this is because (a) komatiites are always intrinsically altered

113   with a significant proportion of their phenocrystic olivine having been fractured and replaced by

114   serpentine, and (b) melt inclusions entrapped during rapid growth of the spinifex olivine often

115   remain connected to groundmass so that their volatile concentrations can be biased by shallow

depth magma degassing. Recently, Shimizu et al. (2009) and Kamenetsky et al. (2010) described volatile-enriched melt inclusions in spinel and olivine from Gorgona komatiitic lavas, with contrasting interpretations. In particular, strong enrichment in volatile elements (CO_2, F, H_2O and Cl) accompanied by high and variable $H_2O/Ce = 307 \pm 198$, $Cl/K_2O = 1.07 \pm 0.52$ ratios (in spinel-hosted melt inclusions) and by exceptionally high H_2O/Ce ratios of 2000−5000 (in olivine-hosted melt inclusions) were assigned to "seawater/brine assimilation" by the magma at upper mantle depth (Shimizu et al., 2009). In contrast, Kamenetsky et al. (2010) suggested the origin of similar volatile-rich olivine-hosted melt inclusions due to partial melting of a wet mantle plume, resulting in a parental komatiitic magma with ~17 wt.% MgO and up to 1.0 wt.% H_2O, whose crystallization occurred at temperatures as low as 1330−1340°C.

Here, we extend our study and report new boron isotope data coupled with volatile and trace element concentrations obtained for a subset of homogenized melt inclusions reported by Kamenetsky et al. (2010). The central purpose of the present work is to shed more light on the origin of the Gorgona komatiitic magmas. These results can be used to better understand the origin of the Caribbean Large Igneous Province as well as that of komatiitic volcanism worldwide.

1.1. Why boron isotopes?

The light lithophile element boron is a very powerful tracer for crust recycling, slab−mantle wedge interaction or shallow depth contamination because boron has no natural redox chemistry and fractionation between the two isotopes of boron is almost entirely controlled by their partitioning between trigonal (near-neutral aqueous fluids preferentially containing [11]B) and tetrahedral species (coordination of B in many silicates, which preferentially incorporate [10]B) (Palmer et al., 1987, 1992; Palmer and Swihart, 1996; Peacock and Hervig, 1999; Williams et al., 2001; Hervig et al., 2002; Tonarini et al., 2003; Schmidt et al., 2005; Wunder et al., 2005). The surface reservoirs are enriched in boron, from 2 ± 1 µg/g B in the lower continental crust through 10−15 µg/g B in the upper crust to ~100 µg/g B in the altered oceanic crust and marine sediments (Harder, 1978; Truscott et al., 1986; Spivack and Edmond, 1986; Leeman et al., 1992; Ishikawa and Nakamura, 1992, 1993; Smith et al., 1995, 1997;

Kasemann et al., 2001; Savov et al., 2009), as compared to the Earth mantle having 0.05–0.25 µg/g B (Ryan and Langmuir, 1993; Chaussidon and Jambon, 1994; Chaussidon and Marty, 1995).

Boron isotopes significantly fractionate during surface geochemical processes (δ^{11}B expressed relatively to NBS 951 standard range from −30 to +60‰ in natural samples from different geological environments; Palmer and Swihart, 1996). Their fractionation is negligible during high-temperature igneous processes, such as partial melting and fractional crystallization, because (a) boron is an incompatible element and remains mostly in the melt (Chaussidon and Libourel, 1993; Chaussidon and Jambon, 1994) and (b) the isotopic fractionation factor ($\alpha_{trigonal-tetrahedral} = [^{11}B/^{10}B]_{trigonal}/[^{11}B/^{10}B]_{tetrahedral}$), as first demonstrated by Kotaka (1973) and Kakihana et al. (1977) using the example of B(OH)$_3$ (boric acid) and [B(OH)$_4$]$^-$ species in the aqueous solutions, decreases strongly from 1.0193 at 300 K to 1.00704 at 700 K but stays nearly constant at higher, magmatic temperatures (1.00393 at 1000 K and 1.00188 at 1500 K). Several "second-order" effects (e.g., differences in geometries and bonding energies between [BO$_4$]-tetrahedra in micas and [B(OH)$_4$]$^-$ species in fluids, presence of various, chemically different species of boron associated with K, Al, and Si complexes in melts and fluids at high pressures and temperatures) can also play an important role in fractionation of B isotopes (Tonarini et al., 2003; Schmidt et al., 2005; Wunder et al., 2005).

Boron isotopic composition of fresh basalts is variable, ranging from −9.4 ± 4.0‰ in the mafic continental rift lavas through −7.3 ± 4.0‰ in oceanic island basalts (OIB) and −3.3 ± 2.2‰ in mid-ocean ridge basalts (MORB) to −0.8 ± 5.0‰ in back arc basin basalts (BABB) (Chaussidon and Jambon, 1994; Chaussidon and Marty, 1995). Later, strongly negative δ^{11}B values of −7.2‰ in the Central Andes and −17.9‰ in Ecuadorian arc lavas were described by Rosner et al. (2003) and Le Voyer et al. (2008). The δ^{11}B value of −10 ± 2‰ has been estimated for the OIB mantle source, and −4.0 ± 1.6‰ and −3.6 ± 1.9‰ for the N-MORB and E-MORB mantle sources, respectively (Chaussidon and Marty, 1995). However, somewhat higher values inferred for the N- and E-MORB sources obtained on the basis of pillow rim glass compositions were explained by probable interaction of the magmas with oceanic crust. Later, Gurenko and

173 Chaussidon (1997) demonstrated the overall ^{11}B-depleted signature of the Icelandic mantle (δ^{11}B

174 $= -11.3 \pm 1.9‰$), based on a study of very primitive olivine-hosted melt inclusions.

175   Systematically higher δ^{11}B values reported for arc lavas compared to exhumed

176 subduction related metamorphic rocks suggest that dehydration reactions significantly decrease

177 the δ^{11}B values of the subducting oceanic crust and sediments, implying strong fractionation of

178 ^{11}B and ^{10}B isotopes as boron partitions in the fluid (Peacock and Hervig, 1999). In particular,

179 this is supported by experimental study of Wunder et al. (2005), which has shown that a wide

180 range of δ^{11}B values in volcanic arcs may result from continuous dehydration of micas. Another

181 major carrier of boron, also a source of variable but generally positive δ^{11}B values, is the

182 serpentinized mantle wedge at the slab-mantle interface (e.g., Benton et al., 2001; Savov et al.,

183 2005, 2007). In relation to these sources of B, the formation of a hydrated wedge due to

184 infiltration of B-rich fluids progressively released from the down dragged slab at arc front depths

185 may account for strongly varying crossarc boron isotopic signatures (Straub and Layne, 2002).

186 On the other hand, Chaussidon and Jambon (1994), Chaussidon and Marty (1995) and Smith et

187 al. (1995) have demonstrated that positive δ^{11}B values accompanied by elevated δ^{18}O of >5.5‰

188 and increasing radiogenic Sr isotope ratios in primitive MORB and OIB magmas can result from

189 shallow-level assimilation of the oceanic crust, whereas the negative δ^{11}B related with relatively

190 low δ^{18}O values of <5.5‰ can be due to interaction of these magmas with the Layer 3 gabbroic

191 crust (for reference, see oxygen isotope profile through the altered, sediment-covered oceanic

192 crust of the Oman ophiolite; Gregory and Taylor, 1981). Finally, B isotope variations from -8.9

193 to $-0.8‰$ in the Snake River Plain−Yellowstone rhyolites can be ascribed to the existence of

194 distinctive sources of boron coming from either juvenile basalt-derived protoliths sitting in the

195 crust or from strongly fluid-depleted, metamorphosed continental crust (Savov et al., 2009). All

196 of the above information suggests that boron isotopes represent a powerful tool which can be

197 effectively used to understand the origin of the Gorgona komatiitic magmas.

198

199 **2. Geological background and studied samples**

200   Gorgona is a small island (8.3 km long and 2.5 km wide) located approximately 50 km to

201 the west off the Pacific coast of Colombia (**Fig. 1**). The geology of Gorgona was first described

202 in Gansser (1950) and Echeverría (1980) and interpreted as a sequence of tilted and faulted

203 blocks of mafic and ultramafic rocks surrounding an axial ridge of cumulate peridotites. The

204 central part of the island is an undeformed peridotite−gabbro complex. Basalts are by far the

205 most abundant eruptive rock type. The komatiite lava flows (1.5 to 6 m thick), often having

206 chilled zones ("polyhedrally jointed zones") at their upper margins, are interlayered with basaltic

207 flows and sills (Kerr, 2005; **Fig. S1a, b;** *Supplementary online material*).

208 The upper polyhedrally jointed layers are usually 20 to 100 cm thick. They contain

209 skeletal olivine microphenocrysts (0.2–0.5 mm) in a very fine grained matrix, grading into a 10

210 to 40 cm thick layer composed of fine random spinifex-textured skeletal olivine plates, set in a

211 groundmass of "feathery" pyroxenes. The spinifex textured layer consist of hollow elongated

212 olivine crystals forming chains, blebby chains and plates up to 50 cm in length, which may be

213 underlain by a thin layer (up to 30 cm thick) of horizontally-oriented, skeletal olivine plates up to

214 10 cm long. Some, not all, flows possess a lower olivine cumulate layer. Where cumulate layers

215 do exist, they are generally thin (20−30 cm) and discontinuous, representing no more than 30%

216 of the flow. The cumulate olivine crystals are up to 1 mm in size, have a predominantly skeletal

217 habit, though polyhedral crystals are also present, and are set in the groundmass composed of

218 radiating needles of clinopyroxene, granular olivine, plagioclase laths and Cr-spinel octrahedra

219 (**Fig. S1c;** *Supplementary online material*).

220 The studied samples were collected from fresh coastal exposures of komatiites on the NE

221 side of the island (**Fig. 1**). Samples GOR94-3/4/17/44 are from the cumulate zone of komatiitic

222 flows, GOR94-28 represents the jointed top of a flow, and GOR94-17 (Punta Trinidad) is from

223 the cumulate zone of a flow having a vesicular zone. The bulk-rock chemical compositions of

224 the studied samples are given in Kamenetsky et al. (2010).

225

226 **3. Results**

227 Olivine hosted melt inclusions (up to 60 µm) have rounded, elliptic to tubular

228 morphologies and appear as either clear glass with a shrinkage bubble or microcrystalline

229 aggregates with several bubbles (**Fig. S1d, e;** *Supplementary online material*). Some inclusions

230 exhibit a visible rim of olivine crystallized on the walls, suggesting extensive post-entrapment

crystallization. Olivine phenocrysts containing melt inclusions were re-heated and homogenized prior to analysis with electron and ion microprobes (for more detail see *Supplementary online material*). The concentrations of major and trace elements and the volatile contents of heated, quenched to glass and corrected for Fe loss melt inclusions were reported by Kamenetsky et al. (2010). Here we present only the composition of melt inclusions which were analyzed for boron isotopes, including several additional inclusions analyzed for volatile and trace elements (**Table 1**).

The inclusions are characterized by relatively high contents of volatile components (0.18–1.03 wt.% H_2O, 0.052–0.077 wt.% S, 0.022–0.031 wt.% Cl) and boron (0.61–2.02 µg/g B), displaying positive anomalies in the overall depleted, primitive mantle (PM) normalized trace element and REE spectra ($[La/Sm]_n$ = 0.16–0.35; $[H_2O/Nb]_n$ = 8–44; $[Cl/Nb]_n$ = 27–68; $[B/Nb]_n$ = 9–30, assuming 300 µg/g H_2O, 8 µg/g Cl and 0.1 µg/g B in PM as normalizing values). The melt inclusions form a compact field of basaltic composition, range from 13 to 18 wt.% MgO, following the common trend of olivine fractionation and accumulation (Fig 2 in Kamenetsky et al., 2010). All inclusions exhibit a very strong enrichment (ca. 10 to 50 times) in H_2O, Cl and B relatively to other trace elements in the multi-element diagram (**Fig. 2**). Their trace element spectra reflect an overall depleted signature ($[La/Sm]_n$ = 0.16–0.38), corresponding to the field of bulk-rock lava compositions.

The B/K ratios ranging from 0.0019 to 0.0063 are systematically higher than those known for primitive N-MORB (B/K of ~0.001) and OIB (B/K of ~0.0003) melt inclusions, pillow rim glasses and lavas (Ryan and Langmuir, 1993; Chaussidon and Jambon, 1994; Gurenko and Chaussidon, 1997). No clear correlations of H_2O, Cl and B contents with other major, trace end especially fluid-mobile incompatible (such as Ba, K, La, Sr) element concentrations are observed. Similarly, the magnitude of B enrichment does not correlate with H_2O or Cl enrichment. We explain this by the very narrow concentration ranges of trace elements in the studied melt inclusions (in particular, 3.1–4.7 µg/g Ba i.e. 12%, 228–343 µg/g K i.e. 11%, 0.5–0.9 µg/g La i.e.13%, and 73–87 µg/g Sr i.e. 5.5% of the average element concentration), which in fact do not exceed the common analytical errors of SIMS measurements for trace elements (the uncertainty ranges between 10 and 30% of 1RSD = 1 relative standard

260 deviation; Kamenetsky et al, 2010). In addition, the absence of correlations may be consistent

261 with a serpentinized arc source of B (and H_2O and Cl) in the included melts which represents, as

262 demonstrated by Savov et al. (2007), "large slab inventory depletions of B (~75%), Cs (~25%),

263 As (~15%), Li (~15%), and Sb (~8%); surprisingly low (generally less than 2%) depletions of

264 Rb, Ba, Pb, U, Sr; and no depletions in REE and the high field strength elements (HFSE)" (see

265 discussion below).

266   The $\delta^{11}B$ values of the studied melt inclusions ranging from −11.5 to +15.6 ‰ at B-

267 concentration of 0.6–2 µg/g also show only subtle correlations with some incompatible elements

268 such as K, Sr, Hf and some REEs, if at all. On the other hand, melt inclusions form two distinct

269 trends based on $\delta^{11}B$ vs. B relationships (**Fig. 3**). The first trend includes seven of 15 inclusions

270 with relatively low $\delta^{11}B$ ranging from −11.5 to −7.3‰ (average −9.0 ± 1.5‰), spanning over the

271 entire range of B concentrations and approaching the "primary" value of the Earth's mantle (−10

272 ± 2‰; Chaussidon and Marty, 1995). Given that igneous processes such as magma fractionation

273 or partial melting do not cause significant fractionation of boron isotopes, we ascribe this trend

274 to olivine crystallization that may occur either in the magma plumbing system or represent

275 incomplete melting of olivine from the inclusion walls during laboratory experiments. The

276 second trend is characterized by extension of $\delta^{11}B$ to highly positive values (up to +15.6‰) with

277 increasing boron concentrations up to 1.6 µg/g B **(Fig. 3)**. Possible reasons of the second trend

278 and its' implications for the origin of Gorgona komatiites are discussed below.

279

280 **4. Discussion**

281 *4.1. Shallow depth magma contamination*

282   A main argument against a hydrous origin of the Gorgona komatiites is their extreme

283 depletion in incompatible trace elements, which progressively increases from basalt through

284 komatiite to picrite, all being related to the same type of the depleted mantle source (e.g., Arndt

285 et al., 1997; Revillon et al., 2000, 2002). In particular, Arndt et al. (1997, p. 297) have noted:

286 "Because the extreme depletion of incompatible elements makes it very unlikely that volatiles

287 were present in the mantle source (they would have been removed along with other incompatible

288 elements during the melt extraction), the parental magma of the tuffs and picrites must have

289 gained water during passage towards the surface, perhaps through assimilation of hydrated crust

290 in a shallow-level magma chamber". Later, Shimizu et al. (2009) described CO_2-rich (40–4000

291 µg/g) komatiitic melt inclusions with highly variable H_2O (0.03–0.9 wt.%) and Cl (6–1056 µg/g)

292 contents in Cr-spinels collected in beach sands from Gorgona. They argued that the volatile

293 contents in melt inclusions could be biased prior to their entrapment by magma degassing or

294 interaction with seawater or brine or, alternatively, by possible post-entrapment modification in

295 the inclusions itself. Our first task is therefore to assess whether the compositional signature of

296 the olivine hosted melt inclusions studied during the present work (i.e., varying B isotope

297 composition, positive H_2O, Cl and B anomalies in the incompatible trace element spectra) could

298 result from shallow depth magma contamination.

299   To answer this question, we examined a two-component mixing scenario, calculating the

300 effects of possible interaction of presumably "uncontaminated" komatiitic magma with seawater,

301 15%- and 50%-NaCl brine and altered oceanic crust in a similar way as it has been done by Kent

302 et al. (1999) and Shimizu et al. (2009). The isotopic composition of boron together with volatile-

303 to-trace or trace-to-trace element ratios (Cl/K_2O, B/K_2O, H_2O/K_2O), as used by Kent et al.

304 (1999) and Shimizu et al. (2009), were selected for model calculations. Due to the lack of data

305 on the composition of altered oceanic crust, marine sediments and other possible contaminating

306 agents specific to the Gorgona region, most of the end-member compositions represent broad

307 estimates available in the submarine environment. We note that the assigned elemental and

308 isotopic compositions of the selected end-members are fixed values taken from literature, though

309 the number of possible contaminants and their compositional range could be more variable. The

310 employment of the advanced assimilation-fractional crystallization model (e.g., DePaolo, 1981)

311 is not applicable to our particular case because all studied melt inclusions were trapped in Mg-

312 rich olivines of Fo_{89-91}, representing very primitive komatiitic magma, which experienced

313 negligible olivine ± Cr-spinel fractionation. Early fractionation of olivine ± spinel cannot

314 significantly affect the volatile contents in the magma since H_2O, Cl, B and K are strongly

315 incompatible in these minerals. Thus, fractionation will cause equivalent enrichment of magma

316 by these elements without affecting their ratios. The following mixing end-members were

317 selected (**Table 2**):

318

1. "Uncontaminated" komatiitic magma. The concentrations of K (309 µg/g), Ba (4.1 µg/g) and Nb (0.44 µg/g) were defined as average composition of seven [11]B-depleted melt inclusions giving average δ^{11}B value of -9.0 ± 1.5‰. The concentrations of H_2O, Cl and B were calculated from the concentrations of neighboring elements of similar incompatibility: $([H_2O]_n = ([La]_n \times [Ce]_n)^{0.5}$, being equal to 0.042 wt.% H_2O, $[Cl]_n = ([Nb]_n \times [K]_n)^{0.5}$, equal to 7.38 µg/g Cl and $[B]_n = ([K]_n \times [La]_n)^{0.5}$, equal to 0.118 µg/g B, so that no enrichment would be visible in the trace element spectra.

2. Seawater. The elemental composition of seawater at 3.5% salinity having 4.5 µg/g B, 19350 µg/g Cl, 392 µg/g K, 0.021 µg/g Ba and 1.5E–05 µg/g Nb was taken from Turekian (1968). Boron isotopic composition (δ^{11}B = +39.5‰) was taken from Leeman and Sisson (1996).

3. 15%- and 50%-NaCl brines. The composition of the brine (15%-NaCl: 85 wt.% H_2O, 99000 µg/g Cl, 2076 µg/g K, 100 µg/g B; 50%-NaCl: 50 wt.% H_2O, 303000 µg/g Cl, 6476 µg/g K) was taken from Kent et al. (1999), who utilized the data of Berndt and Seyfried (1990) obtained for experimental phase-separated brines. The concentrations of Ba = 0.111 µg/g and Nb = 7.94E–05 µg/g in the 15%-NaCl brine and the concentrations of B = 312 µg/g, Ba = 0.347 µg/g and Nb = 2.48E–04 µg/g in the 50%-NaCl brine were calculated by proportional extrapolation of the known concentrations of B in the 15%-NaCl brine given by Kent et al. (1999) and Ba and Nb in seawater to the higher K concentrations by keeping constant their B/K, Ba/K and Nb/K ratios. Boron isotopic composition of natural NaCl brines varies strongly, ranging from +25.5 to +48.7‰ in the brines from the Australian salt lakes and from +55.7 to +57.4‰ in the surface brines of Red Sea, Israel (e.g., Vengosh et al., 1991a, b). We arbitrary assigned the extreme δ^{11}B values of +25.5‰ and +57.4‰ to the 15%- and 50%-NaCl brines, respectively, because, as shown below, such difference in isotopic and trace element composition between 15%- and 50%-NaCl brines only marginally affects the calculation results.

4. Altered oceanic crust (AOC). The chemical composition of AOC, especially that of volatile components, varies strongly between different segments of the ocean floor (e.g.,

347   Michael and Cornell, 1998). These authors demonstrated that MORBs from the

348   Galapagos spreading center have strongly varying Cl and K concentrations (25–4050

349   µg/g Cl, 249–4151 µg/g K; Cl/K = 0.06–1.09). For our modeling, we have chosen the

350   concentrations of Cl and K representing mean values of the above ranges (2040 µg/g Cl

351   and 2200 µg/g K, giving Cl/K = 0.93). The concentrations of Ba = 22.6 µg/g, Nb = 1.22

352   µg/g, H_2O = 5 wt.%, B = 5.2 µg/g and $\delta^{11}B$ = +3.7‰ were taken from Smith et al.

353   (1997), Kent et al. (1999) and Hochstaedter et al. (2001).

354   5. Siliceous marine sediment (SED). The concentrations of K = 1245 µg/g, H_2O = 8.2 wt.%,

355   Ba = 1950 µg/g, and Nb = 2.44 µg/g correspond to the Colombia sediment from

356   DSDP/ODP drill Hole 504 located 200 km south of the Costa Rica Rift in the eastern

357   equatorial Pacific (Table 1 in Plank and Langmuir, 1998). We note that SED end-

358   member was selected exclusively as one possible, if not a single, end-member to account

359   for the negative $\delta^{11}B$ ratios in ^{11}B-depleted melt inclusions. In contrast to marine

360   carbonates, which are usually characterized by positive and wide range of $\delta^{11}B$ from ~0

361   to +30‰, the terrigenous, siliceous sediments may have $\delta^{11}B$ as low as –15‰ (Leeman

362   and Sisson, 1996 and references therein). In particular, the concentration of B = 120 µg/g

363   and $\delta^{11}B$ = –10‰ (Smith et al., 1997) were assigned to SED. Although the

364   concentrations of Cl in marine sediments are expected to be strongly varying, we also

365   arbitrary assigned 1000 µg/g Cl to SED because, as stated above, Cl does not play an

366   essential role in our calculations, and the SED mixing lines on the diagrams, except to

367   one panel outlining relationships between $\delta^{11}B$ and B/K_2O, are given only for

368   comparison with other mixing end-members.

369

370   As follows from the modeling (**Fig. 4**), direct contamination of the ascending komatiitic

371 magma at shallow depth by crustal rocks, as suggested by Arndt et al. (1997), or by seawater or

372 seawater-derived components (saline brines; Shimizu et al., 2009), is unable to account for the

373 H_2O, Cl and B enrichment observed in the studied melt inclusions. We emphasize that if one

374 would consider mixing relations in coordinates of Cl/K_2O vs. H_2O/K_2O ratios only, following

375 Shimizu et al. (2009), such an approach may lead to an erroneous conclusion. Indeed, to account

376   for the compositions of melt inclusions with $H_2O/K_2O = 4.5–29.6$, $Cl/K_2O = 0.46–1.04$, would

377   require <1.5 wt.% seawater or even <0.7 wt.% of 15%-NaCl brine or <0.2 wt.% of 50%-NaCl

378   brine, respectively (**Fig. 4a**). No effect of AOC or oceanic sediments can be recognized in this

379   diagram. Similarly, mixing the komatiite end-member with 0.5–1.8 wt.% of 15%-NaCl brine or

380   0.2–0.5 wt.% of 50%-NaCl brine may effectively explain the entire range of B/K_2O ratios found

381   in the studied melt inclusions. In contrast, if we plot the results of this mixing in coordinates of

382   B/K_2O vs. Cl/K_2O (**Fig. 4c**), the essential role of seawater, 15%- and 50%-NaCl brines (the most

383   effective contamination agents in **Fig. 4a, b)**, as well as the role of altered oceanic crust and

384   marine sediments are no longer justified. Mixing relations in coordinates $\delta^{11}B$ vs. B/K_2O (**Fig.**

385   **4d**) also provide no evidence for magma contamination. Although admixture of marine

386   sediments (less than 2 wt.% of SED) to the komatiitic magma may potentially account for the

387   $\delta^{11}B$ range in the ^{11}B-depleted melt inclusions, we rule out this possibility because there is no

388   evidence for a significant role of marine sediments from the volatile-trace element relations (**Fig.**

389   **4a-c**). In conclusion, we note that our data are also in a good agreement with Walker et al. (1999,

390   p. 722) who have concluded: "Although, the most radiogenic Gorgona komatiites have the

391   lowest Os concentrations in the suite, mass balance arguments weigh heavily against lithospheric

392   contamination of their parental magmas accounting for the enrichments in ^{187}Os".

393

394   *4.2. Fluid-induced mantle melting: was it due to subduction impact?*

395   Since shallow contamination of the Gorgona komatiitic magmas can not account for

396   volatile enrichment in the melt inclusions, implying a primary juvenile origin of H_2O, Cl and B

397   (Kamenetsky et al., 2010), another process capable of changing B isotopic composition in the

398   included melts, but not major and trace element concentrations, has to be investigated. Relatively

399   high H_2O and Cl abundances in komatiitic melt inclusions have previously been reported for the

400   Belingwe komatiites, Zimbabwe (0.18–0.26 wt.% H_2O, Danyushevsky et al., 2002b; 1.1–1.7

401   wt.% H_2O, Shimizu et al., 2001; 0.4–0.6 wt.% H_2O, 500–700 µg/g Cl, Cl/K_2O ~0.8–1.5, Kent et

402   al., 2009). In particular, Kent et al. (2009) have suggested generation of the Belingwe komatiitic

403   magmas "from melting of ″damp″ mantle, possibly with analogies to modern back arc

404   environments".

405   Although the model proposing that komatiites are generated by dry and hot mantle

406   plumes rising from the thermal boundary layer within the Earth is widely recognized (Arndt et

407   al., 1997; Herzberg, 1995; Kerr, 2005; Kerr et al., 1995, 1996; Walter, 1998; Révillon et al.,

408   2000, 2002; Hastie and Kerr, 2010), an alternative scenario which favors a subduction related

409   origin, recently reviewed in detail by Parman and Grove (2005), apparently could be viable to

410   explain substantial H_2O contents found in several types of komatiites, including those from the

411   Island of Gorgona studied here. As stated above, a recent set of ^{40}Ar-^{39}Ar ages obtained for the

412   main types of Gorgona mafic rocks (Serrano et al., 2011) documents much longer magmatic

413   activity on the island (from 98.7 ± 7.7 to 61.4 ± 4.8 Ma), as compared to the previous age

414   determinations of about 86−92 Ma (Aitken and Echeverría, 1984; Sinton et al., 1998; Walker et

415   al., 1999). Serrano et al. (2011) concluded that the diffuse magmatism occurred in Gorgona

416   Island shows no clear pattern of migration, being broadly coeval with the opening of the

417   Caribbean slab window and question, in fact, the broadly accepted origin of the Caribbean LIP

418   ultimately due to melting of a plume head at ~90Ma. Then, if the model advocated by Serrano et

419   al. (2011) is correct, the fluids released from the subducting slab or from metasomatically

420   reworked mantle wedge might have triggered partial melting in the upwelling mixed mantle,

421   resulting in a wide compositional range of magmas variously enriched or depleted in volatile

422   components and having a range of $\delta^{11}B$ values. This scenario is in agreement with the recent

423   study of Kamenetsky et al. (2010), who also have questioned the ultimately "hot" signature of

424   the Gorgona komatiites.

425   A significant fraction of initial boron and ^{11}B isotope inventory is contained in the

426   uppermost few km of the subducting oceanic crust and sediments, being released progressively

427   as subduction proceeds (e.g., Leeman and Sisson, 1996). Boron mobilized from the slab due to

428   its dehydration will be systematically heavier than the parental AOC, resulting in +5 to +10‰

429   enrichment of the fluid at 400−500°C (Ishikawa and Nakamura, 1992; Leeman and Sisson, 1996;

430   Rose et al. 2001, Rosner et al. 2003; Leeman et al., 2004; Le Voyer et al., 2008). Since the

431   composition of slab-derived fluid may vary strongly, depending closely on the composition of

432   the subducting crust, on one hand, and the degree of its devolatilization, on another, a wide $\delta^{11}B$

433   range from −7‰ through +2‰ up to +15‰ (assuming +10‰ enrichment of the fluid phase

relative to the upper end of $\delta^{11}B$ values given for AOC by Smith et al., 1997) is very probable (Rose et al. 2001; Leeman et al., 2004; Gurenko et al., 2005; Le Voyer et al., 2008; Tonarini et al., 2011 and references therein). The recent study by Tonarini et al. (2011) reports boron isotope data for the South Sandwich Island arc lavas, emphasizing their very positive $\delta^{11}B$ values (+12 to +18‰, being the heaviest yet observed for subduction-related rocks), substantial enrichment in B concentrations (3 to 25 µg/g B) and decoupling of B from other fluid-immobile incompatible elements. All these signatures are very similar to what we observe for the Gorgona melt inclusions, except for relatively high B concentrations. The authors propose multi-stage recycling of high-$\delta^{11}B$ and high-B serpentinite (mixed with arc crust and sediment material) as a possible source of extremely ^{11}B-rich fluids. Presence of serpentinite in the slab is particularly important because (a) minimal B isotopic fractionation is expected during breakdown of serpentinite minerals, (b) high-$\delta^{11}B$ and high-B concentration fluids can be hosted in serpentine minerals up to 3–4 GPa and 650 °C and (c) when released, these fluids may account for decoupling of B and trace elements such as Rb, Ba, Pb, U, Sr (Ulmer and Trommsdorff, 1995; Benton et al., 2001; Savov et al., 2005, 2007; Tonarini et al., 2011).

Similar processes of fluid-enhanced partial melting of a hot mantle plume can be considered to account for the $\delta^{11}B$ range in the Gorgona melt inclusions. The effects of possible interaction of slab-derived fluids with depleted MORB-like mantle source are illustrated on diagrams in coordinates of $\delta^{11}B$ vs. B/Nb and Ba/Nb ratios (**Fig. 5**). Given that $^{10}B/^{11}B$, B/Nb and Ba/Nb ratios do not change significantly during partial melting or magma crystallization processes, the ratios of these elements calculated for the source can be directly applied to the resulting partial melts. The mixing end-members were defined as below (**Table 2**):

1. Mantle (MANT). A depleted trace element and radiogenic isotope signature of the Caribbean plume giving rise to the Gorgona komatiites has been proposed by Arndt et al. (1997). Taking into account the overall trace element depleted composition of the studied melt inclusions, a depleted MORB-like mantle component containing 1.2 µg/g Ba, 0.21 µg/g Nb, 0.06 µg/g B but having $\delta^{11}B = -10‰$ (Chaussidon and Marty, 1995; Salters and Stracke, 2004) has been selected.

463   2. Recycled crust (REC). The concentrations of trace elements and B in the recycled crust,

464   whose potential presence in the source of the Gorgona komatiites can be deduced from

465   Re-Os isotope systematics (Walker et al., 1991, 1999), was taken to be the same as that

466   of AOC previously used in modeling. The B isotopic composition of REC was fixed at

467   −12.8‰, corresponding to $\delta^{11}B$ value of the residual slab (Tonarini et al., 2011).

468   3. Serpentinite (SERP). The forearc serpentinized peridotites are characterized by a wide

469   range of boron contents (6.6–126 µg/g B), boron isotopic composition (+10.4 to

470   +25.3‰) and trace element concentrations (Benton et al., 2001; Savov et al., 2005,

471   2007). The presence of a serpentinized mantle wedge at the slab-mantle interface and its

472   admixture into the ascending hot mantle plume may potentially modify the composition

473   of the source rocks whereas the plume penetrates through a gap in the slab. We thus

474   consider serpentinized peridotite as a possible mixing end-member, assigning the

475   following composition: 3.2 µg/g Ba, 0.1 µg/g Nb, 20 µg/g B and $\delta^{11}B$ = 14.8‰ based on

476   the data by Benton et al. (2001) and Savov et al. (2005, 2007).

477   4. Subducting slab fluid (SSF). Three subducting slab fluid compositions (SSF1 through

478   SSF3) with contrasting B concentrations and isotopic compositions (SSF1: 1000 µg/g Ba,

479   200 µg/g B, $\delta^{11}B$ = 15‰; SSF2: 500 µg/g Ba, 100 µg/g B, $\delta^{11}B$ = 2‰; SSF3: 250 µg/g

480   Ba, 50 µg/g B, $\delta^{11}B$ = −7‰ at constant Nb = 0.36 µg/g) were compiled based on the

481   Rosner et al. (2003), Leeman et al. (2004), Gurenko et al. (2005), Le Voyer et al. (2008)

482   and Tonarini et al. (2011) data. The decrease of B and Ba contents and $\delta^{11}B$ values in the

483   fluid components qualitatively reflects the increase of slab temperature and degree of its

484   devolatilization. We note that the fluids released from ultramafic slab ± serpentinite and

485   recycled forearc serpentinites (Tonarini et al., 2011) are within the range of SSF1 to

486   SSF3 compositions currently used and thus not considered as individual end-members.

487

488   As follows from the calculations, the major agent affecting the chemical composition of

489 the hybrid mantle source and, consequently, the magmas formed by its partial melting is the

490 composition of a fluid component released from the slab (in the case of subduction related

491 scenario) or the composition of the crust in the magma source (recycling scenario). The presence

492   of ancient recycled crust in the source region (~10%, depending on the B/Nb or Ba/Nb variables

493   used; **Fig. 5**), is possible but accounts only for a restricted part of the most δ^{11}B-depleted melts.

494   On the other hand, this amount is in a very good agreement with Re-Os isotopic data of Walker

495   et al. (1999), who proposed that only a minor amount (<10%) of the recycled material might be

496   present in the source of Gorgona komatiites. The role of serpentinized peridotites, which may

497   occasionally be entrained by the hot rising plume, is also limited. These may account only for the

498   most δ^{11}B-enriched melts, requiring 1–10% of admixture.

499   The injection of the slab-derived fluids into melting region appears to be the most

500   effective mechanism, as for producing B isotope variability because there is a wide range of δ^{11}B

501   and B/Nb and Ba/Nb ratios in the fluid phase, as for decreasing the temperature of peridotite

502   solidus. Less than 1 wt.% of SSF1 or SSF2 fluid has to be injected in the ascending hot mantle

503   material in order to explain the observed δ^{11}B enrichment up to ~16‰. The majority of low-δ^{11}B

504   melt inclusions would require admixture of less that 3 wt.% of the SSF3 fluid, representing the

505   most high temperature product of slab devolatilization. We note that such a small amount of this

506   fluid will not result in a significant enrichment in fluid mobile incompatible trace elements, such

507   as Ba, B (both used in calculation), K, La, Ce and Sr, which are typical in subduction-related

508   magmas, and thus may argue for the immediate role of subduction-derived aqueous fluids in the

509   origin of H_2O, Cl and B enrichment. Finally, our data support the conclusion by Kamenetsky et

510   al. (2010) who demonstrated that in the presence of 0.2–1.0 wt.% H_2O in the melt, the initial

511   crystallization temperature of the Gorgona komatiitic magma could be as low as 1330–1340°C,

512   though being still higher than the temperature of common mid-ocean ridge magmas.

513

514   **5. Conclusions**

515   1. The olivine-hosted melt inclusions from Gorgona komatiites are characterized by a wide

516   range of δ^{11}B values from −11.5 to +15.6 ± 2.2‰ (1 SE), forming two distinct trends as a

517   function of B concentration. The first major trend includes melts with relatively low and

518   constant δ^{11}B values ranging from −11.5 to −7.3‰ (giving an average of −9.0 ± 1.5‰),

519   while the second trend shows a drastic increase of δ^{11}B up to +15.6‰, at similar but

520   varying (0.6–2 µg/g) concentrations of B.

521   2. Direct assimilation of seawater, seawater-derived components, altered oceanic crust or

522   marine sediments by ascending komatiite magma cannot readily account for the volatile

523   contents and B isotope variations.

524   3. Injection of the subduction slab fluid into the rising mantle plume in amount of <3 wt.%

525   provides a plausible explanation for the $\delta^{11}B$ range, and also may explain the origin of

526   H_2O, Cl and B enrichment of the Gorgona olivine hosted melt inclusions and slightly

527   elevated, as compared to MORB, but still relatively low initial temperatures of the

528   Gorgona komatiite magmas (Kamenetsky et al., 2010).

529

545

546

547   **References**

548   Allègre, C.J., 1982. Genesis of Archean komatiites in a wet ultramafic subducted plate. In:

549   Arndt, N., Nisbet, E.G. (Eds.) Komatiites. Berlin, Springer-Verlag, 495−500.

550   Arndt, N.T., Kerr, A.C., Tarney, J., 1997. Dynamic melting in plume heads: The formation of

551   Gorgona komatiites and basalts. Earth Planet. Sci. Lett. 146, 289−301.

552   Arndt, N., Ginibre, C., Chauvel, C., Albarède, F., Cheadle, M., Herzberg, C., Jenner, G., Lahaye,

553   Y., 1998. Were komatiites wet? Geology 26, 739−742.

554   Aitken, B.G., Echeverría, L.M., 1984. Petrology and geochemistry of komatiites and tholeiites

555   from Gorgona Island, Colombia. Contrib. Mineral. Petrol. 86, 94−105.

556   Benton, L.D., Ryan, J.G., Tera, F., 2001. Boron isotope systematics of slab fluids as inferred

557   from a serpentine seamount, Mariana forearc, Earth Planet. Sci. Lett. 187, 273−282.

558   Berndt, M.E., Seyfried, W.E.J., 1990. Boron, bromine, and other trace elements as clues to the

559   fate of chlorine in mid-ocean ridges. Geochim. Cosmochim. Acta 54, 2235−2245.

560   Berry, A.J., Danyushevsky, L.V., O'Neill, H.St.C., Newville, M., Sutton, S.R., 2008. Oxidation

561   state of iron in komatiitic melt inclusions indicates hot Archaean mantle. Nature 455,

562   960−963.

563   Chaussidon, M., Libourel, G., 1993. Boron partitioning in the upper mantle: An experimental

564   and ion probe study. Geochim. Cosmochim. Acta 57, 5053−5062.

565   Chaussidon, M., Jambon, A., 1994. Boron content and isotopic composition of oceanic basalts:

566   geochemical and cosmochemical implications. Earth Planet. Sci. Lett. 121, 277−291.

567   Chaussidon, M., Marty, B., 1995. Primitive boron isotope composition of the mantle. Science,

568   269, 383−386.

569   Danyushevsky, L.V., McNeill, A.W., Sobolev, A.V., 2002a. Experimental and petrological

570   studies of melt inclusions in phenocrysts from mantle-derived magmas: an overview of

571   techniques, advantages and complications: Chem. Geol. 183, 5−24.

572   Danyushevsky, L.V., Gee, M.A.M., Nisbet, E.G., and Cheadle, M.J., 2002b. Olivine-hosted melt

573   inclusions in Belingwe komatiites: Implications for cooling history, parental magma

574   composition and its H_2O content. Geochim. Cosmochim. Acta 66, A168.

575   DePaolo, D.J., 1981. Trace element and isotopic effects of combined wallrock assimilation and

576   fractional crystallization. Earth Planet. Sci. Lett. 53, 189−202.

577   Dixon, J.E., Clague, D.A., Stolper, E.M., 1991. Degassing history of water, sulfur and carbon in

578   submarine lavas from Kilauea volcano, Hawaii. J. Geol. 99, 371−394.

579   Echeverría, L.M., 1980. Tertiary or Mesozoic komatiites from Gorgona island, Colombia: field

580   relations and geochemistry. Contrib. Mineral. Petrol. 73, 253– 266.

581   Echeverría, L.M., Aitken, B.G., 1986. Pyroclastic rocks: Another manifestation of ultramafic

582   volcanism on Gorgona Island, Colombia. Contrib. Mineral. Petrol. 92, 428–436.

583   Gansser, A., 1950. Geological and petrological notes on Gorgona island in relation to north-west

584   S America. Schweiz. Mineral. Petrograph. Mitt. 30, 219– 237.

585   Gregory, R.T., Taylor, H.P., 1981. An oxygen isotope profile in a section of Cretaceous oceanic

586   crust, Samail ophiolite, Oman: evidence for δ^{18}O buffering of the oceans by deep (>5 km)

587   seawater-hydrothermal circulation at mid-ocean ridges. J. Geophys. Res. 86, 2737−2755.

588   Grove, T.L., Parman, S.W., 2004. Thermal evolution of the Earth as recorded by komatiites.

589   Earth Planet. Sci. Lett. 219, 173−187.

590   Gurenko, A.A., Chaussidon, M., 1995. Enriched and depleted primitive melts included in olivine

591   from Icelandic tholeiites: origin by continuous melting of a single mantle column. Geochim.

592   Cosmochim. Acta 59, 2905−2917.

593   Gurenko, A.A., Chaussidon, M., 1997. Boron concentrations and isotopic composition in the

594   Icelandic mantle: evidence from glass inclusions in olivine. Chem. Geol. 135, 21−34.

595   Gurenko, A.A., Trumbull, R.B., Thomas, R., Lindsay J.M., 2005. A melt inclusion record of

596   volatiles, trace elements and Li-B isotope variations in a single magma system from the Plat

597   Pays Volcanic Complex, Dominica, Lesser Antilles. J. Petrol. 46, 2495−2526.

598   Harder, H., 1978. Boron: granitic rocks and related effusives. In: Wedepohl, K.H., (Ed.),

599   Handbook of geochemistry, II-1. Springer Verlag, Berlin, 5E5−5E10.

600   Hastie, A.R., Kerr, A.C., 2010. Mantle plume or slab window?: Physical and geochemical

601   constraints on the origin of the Caribbean oceanic plateau. Earth-Sci. Rev. 98, 283−293.

602   Herzberg, C., 1995. Generation of plume magmas through time: an experimental perspective.

603   Chem. Geol. 126, 1–16.

604   Herzberg, C., Asimow, P.D., Arndt, N., Niu, Y., Lesher, C.M., Fitton, J.G., Cheadle, M.J.,
605   Saunders, A.D., 2007. Temperatures in ambient mantle and plumes: Constraints from
606   basalts, picrites, and komatiites. Geochem. Geophys. Geosyst. 8,
607   DOI:10.1029/2006GC001390.

608   Hervig, R.L., Moore, G.M., Williams, L.B., Peacock, S.M., Holloway, J.R., Roggensack, K.,
609   2002. Isotopic and elemental partitioning of boron between hydrous fluid and silicate melt.
610   Amer. Mineral. 87, 769– 774.

611   Hochstaedter, A., Gill, J., Peters, R., Broughton, P., Holden, P., Taylor, B., 2001. Across-arc
612   geochemical trends in the Izu-Bonin arc: Contributions from the subducting slab. Geochem.
613   Geophys. Geosyst. 2, 2000GC000105.

614   Hofmann, A.W., 1988. Chemical differentiation of the Earth: the relationship between mantle,
615   continental crust and oceanic crust. Earth Planet. Sci. Lett. 90, 297−314.

616   Ishikawa, T., Nakamura, E., 1992. Boron isotope geochemistry of the oceanic crust from
617   DSDP/ODP hole 504B. Geochim. Cosmochim. Acta 56, 1633−1639.

618   Ishikawa, T., Nakamura, E., 1993. Boron isotope systematics of marine sediments. Earth Planet.
619   Sci. Lett. 117, 567−580.

620   Jarosewich, E.J., Nelen, J.A., Norberg, J.A., 1980. Reference samples for electron microprobe
621   analysis. Geostand. Newslett. 4, 43−47.

622   Kakihana, H., Kotaka, M., Satoh, S., Nomura, M. Okamoto, M, 1977. Fundamental studies on
623   the ion-exchange separation of boron isotopes. Bull. Chem. Soc. Japan 50, 158−163.

624   Kamenetsky, V.S., Gurenko, A.A., Kerr, A.C., 2010. Composition and temperature of komatiite
625   melts from Gorgona Island constrained from olivine-hosted melt inclusions. Geology 38,
626   1003–1006.

627   Kasemann, S., Meixner, A., Rocholl, A., Vennemann, T., Rosner, M., Schmitt, A., Wiedenbeck,
628   M., 2001. Boron and oxygen isotope composition of certified references materials NIST
629   SRM 610/612 and reference materials JB-2 and JR-2. Geostand. Newslett.: J. Geostand.
630   Geoanalys. 25, 405– 416.

631   Kent, A.J.R., Norman, M.D., Hutcheon, I.D., Stolper, E.M., 1999. Assimilation of seawater-

632   derived components in an oceanic volcano: evidence from matrix glasses and glass

633   inclusions from Loihi seamount, Hawaii. Chem. Geol. 156, 299−319.

634   Kent, A.J.R., Hauri, E., Woodhead, J., Hergt, J.M., 2009. Volatile contents of Belingewe

635   komatiites: Mantle volatile contents and the effects of degassing, Geochim. Cosmochim.

636   Acta 73, A640.

637   Kerr, A.C., 2005. La Isla de Gorgona, Colombia: A petrological enigma? Lithos 84, 77−101.

638   Kerr, A.C., Saunders, A.D., Tarney, J., Berry N.H., Hards, V.L., 1995. Depleted mantle plume

639   geochemical signatures: no paradox for plume theories, Geology 23, 843–846.

640   Kerr, A.C., Marriner, G.F., Arndt, N.T., Tarney, J., Nivia, A., Saunders, A.D., Duncan, R.A.,

641   1996. The petrogenesis of Gorgona komatiites, picrites and basalts: new field, petrographic

642   and geochemical constraints. Lithos 37, 245−260.

643   Kotaka, M., 1973. Chromatographic separation of boron and nitrogen isotopes using pure water

644   as eluent. Ph.D. Dissertation, Tokyo Inst. Tech., 163 pp.

645   Leeman, W.P., Sisson, V.B., 1996. Geochemistry of boron and its implications for crustal and

646   mantle processes. In: Grew, E.S., Anovitz, L.M. (Eds.) Boron: Mineralogy, Petrology and

647   Geochemistry. Rev. Mineral., Mineral. Soc. Am., Washington, DC, 33, 645−707.

648   Leeman, W.P., Sisson, V.P., Reid, M.R., 1992. Boron geochemistry of the lower crust: Evidence

649   from granulite terranes and deep crustal xenoliths. Geochim. Cosmochim. Acta 56,

650   775−788.

651   Leeman, W.P., Tonarini, S., Chan, L.H., Borg, L.E., 2004. Boron and lithium isotopic variations

652   in a hot subduction zone—the southern Washington Cascades. Chem. Geol. 212, 101−124.

653   Le Voyer, M., Rose-Koga, E.F., Laubier, M., Schiano, P., 2008. Petrogenesis of arc lavas from

654   the Rucu Pichincha and Pan de Azucar volcanoes (Ecuadorian arc): Major, trace element,

655   and boron isotope evidences from olivine-hosted melt inclusions. Geochem. Geophys.

656   Geosyst. 9, DOI:12010.11029/12008GC002173.

657   Litasov, K., Ohtani, E., 2002. Phase relations and melt compositions in CMAS-pyrolite-H_2O

658   system up to 25 GPa. Phys. Earth Planet. Inter. 134, 105−127.

659 McDonough, W.F., Ireland, T.R., 1993. Intraplate origin of komatiites inferred from trace
660   elements in glass inclusions: Nature 365, 432–434.

661 Michael, P.J., Cornell, W.C., 1998. Influence of spreading rate and magma supply on
662   crystallization and assimilation beneath mid-ocean ridges: Evidence from chlorine and
663   major element chemistry of mid-ocean ridge basalts. J. Geophys. Res. 103, 18325–18356.

664 Palmer, M.R., Swihart, G.H., 1996. Boron isotope geochemistry: an overview. In: Grew, E.S.,
665   Anovitz, L.M. (Eds.), Boron: Mineralogy, Petrology and Geochemistry. Rev. Mineral.,
666   Mineral. Soc. Am., Washington, D.C., 33, 709−744.

667 Palmer, M.R., Spivack, A.J., Edmond, J.M., 1987. Temperature and pH controls over isotopic
668   fractionation during adsorption of boron on marine clay. Geochim. Cosmochim. Acta 51,
669   2319–2323.

670 Palmer, M.R., London, D., Morgan VI, G.B., Babb, H.A., 1992. Experimental determination of
671   fractionation of $^{11}B/^{10}B$ between tourmaline and aqueous vapor: a temperature- and
672   pressure-dependent isotopic system. Chem. Geol. 101, 123– 129.

673 Parman, S.W., Grove, T.L., 2005. Komatiites in the plume debate. In: Foulger, G.R., Natland,
674   J.H., Presnallm D.C., Anderson, D.L. (Eds.), Plates, Plumes, and Paradigms, GSA Special.
675   Publ. 388, 249−256.

676 Parman, S.W., Dann, J.C., Grove, T.L., de Wit, M.J., 1997. Emplacement conditions of
677   komatiite magmas from the 3.49 Ga Komati Formation, Barberton Greenstone Belt. South
678   Africa Earth Planet. Sci. Lett. 150, 303−324.

679 Peacock, S.M., Hervig, R.L., 1999. Boron isotopic composition of subduction-zone metamorphic
680   rocks. Chem. Geol. 160, 281– 290.

681 Pindell, J.L., Kennan, L., 2009. Tectonic evolution of the Gulf of Mexico, Caribbean and
682   northern South America in the mantle reference frame: an update. In: James, K., Lorente,
683   M.A., Pindell, J. (Eds.), The geology and evolution of the region between North and South
684   America. Geol. Soc. London, Special. Publ. 328, 1–55.

685 Pindell, J.L., Kennan, L., Stanek, K.P., Maresch, W.V., Draper, G.G., 2006. Foundations of Gulf
686   of Mexico and Caribbean evolution: Eight controversies resolved. Acta Geologica 4, 303–
687   341.

688   Plank, T., Langmuir, C.H., 1998. The chemical composition of subducting sediment and its
689   consequences for the crust and mantle. Chem. Geol. 145, 325−394.

690   Révillon, S., Arndt, N.T., Chauvel, C., Hallot, E., 2000. Geochemical study of ultramafic
691   volcanic and plutonic rocks from Gorgona Island, Colombia: The plumbing system of an
692   oceanic plateau. J. Petrol. 41, 1127−1153.

693   Révillon, S., Chauvel, C., Arndt, N.T., Pik, R., Martineau, F., Fourcade, S., Marty, B., 2002.
694   Heterogeneity of the Caribbean plateau mantle source: Sr, O and He isotopic compositions
695   of olivine and clinopyroxene from Gorgona Island. Earth Planet. Sci. Lett. 205, 91−106.

696   Rose, E.F., Shimizu, N., Layne, G.D., Grove, T.L., 2001. Melt production beneath Mt. Shasta
697   from boron data in primitive melt inclusions. Science 293, 281−283.

698   Rosner, M., Erzinger, J., Franz, G., Trumbull, R.B., 2003. Slab-derived boron isotope signatures
699   in arc volcanic rocks from the Central Andes and evidence for boron isotope fractionation
700   during progressive slab dehydration. Geochem. Geophys. Geosyst. 4,
701   DOI:0.1029/2002GC000438.

702   Ryan, J.G., Langmuir, C.H., 1993. The systematics of boron abundances in young volcanic
703   rocks. Geochim. Cosmochim. Acta 57, 1489−1498.

704   Salters, V.J.M., Stracke, A., 2004. Composition of the depleted mantle. Geochem. Geophys.
705   Geosyst. 5, DOI:10.1029/2003GC000597.

706   Savov, I.P., Ryan, J.G, D'Antonio, M., Kelley, K., Mattie, P., 2005. Geochemistry of
707   serpentinized peridotites from the Mariana Forearc- Conical Seamount, ODP Leg 125:
708   Implications for the elemental recycling at subduction zones. Geochem. Geophys. Geosyst.
709   6, Q04J15, doi:10.1029/2004GC000777.

710   Savov, I.P., Ryan, J.G., D'Antonio, M., Fryer, P., 2007. Shallow slab fluid release across and
711   along the Mariana arc-basin system: Insights from geochemistry of serpentinized peridotites
712   from the Mariana Forearc. J. Geophys. Res. 112, doi:10.1029/2006JB004749.

713   Savov, I.P., Leeman, W.P., Lee, C.T., Shirey, S.B., 2009. Boron isotopic variations in NW USA
714   rhyolites: Yellowstone, Snake River Plain, Eastern Oregon. J. Volcanol. Geotherm. Res.
715   188, 162−172.

716   Schmidt, C., Thomas, R., Heinrich, W., 2005. Boron speciation in aqueous fluids at 22 to 600 °C

717   and 0.1 MPa to 2 GPa. Geochim. Cosmochim. Acta 69, 275– 281.

718   Serrano, L., Ferrari, L., Martínez, M.L., Petrone, C.M., Jaramillo, C., 2011. An integrative

719   geologic, geochronologic and geochemical study of Gorgona Island, Colombia: Implications

720   for the formation of the Caribbean Large Igneous Province. Earth Planet. Sci. Lett.,

721   doi:10.1016/j.epsl.2011.07.011.

722   Shimizu, K., Komiya, T., Hirose, K., Shimizu, N., Maruyama, S., 2001. Cr-spinel, an excellent

723   micro-container for retaining primitive melts − implications for a hydrous plume origin for

724   komatiites. Earth Planet. Sci. Lett. 189, 177−188.

725   Shimizu, K., Shimizu, N., Komiya, T., Suzuki, K., Maruyama, S., Tatsumi, Y., 2009. CO_2-rich

726   komatiitic melt inclusions in Cr-spinels within beach sand from Gorgona Island, Colombia.

727   Earth Planet. Sci. Lett. 288, 33−43.

728   Sinton, C.W., Duncan, R.A., Storey, M., Lewis, J., Estrada, J., 1998. An oceanic flood basalt

729   province at the core of the Caribbean plate. Earth Planet. Sci. Lett. 155, 221−235.

730   Smith, H.J., Spivack, A.J., Staudigel, H., Hart, S.R., 1995. The boron isotope composition of

731   altered oceanic crust. Chem. Geol. 126, 119−135.

732   Smith, H.J., Leeman, W.P., Davidson, J., Spivack, A.J., 1997. The B isotopic composition of arc

733   lavas from Martinique, Lesser Antilles. Earth Planet. Sci. Lett. 146, 303−314.

734   Sobolev AV, Danyushevsky LV (1994) Petrology and geochemistry of boninites from the North

735   Termination of the Tonga Trench: Constraints on the generation conditions of primary high-

736   Ca boninite magmas. J Petrol 35: 1183−1211.

737   Sobolev, A.V., Chaussidon, M., 1996. H_2O concentrations in primary melts from supra-

738   subduction zones and mid-ocean ridges: implications for H_2O storage and recycling in the

739   mantle. Earth Planet. Sci. Lett. 137, 45−55.

740   Spivack, A.J., Edmond, J.M., 1986. Determination of boron isotope ratios by thermal ionization

741   mass spectrometry of the dicesium metaborate cation. Anal. Chem. 58, 31−35.

742   Straub, S.M., Layne, G.D., 2002. The systematics of boron isotopes in Izu arc front volcanic

743   rocks. Earth Planet. Sci. Lett. 198, 25−39.

744 Thordarson, T., Self, S., Oskarsson, N., Hulsebosch, T., 1996. Sulfur, chlorine, and fluorine
745   degassing and atmospheric loading by the 1783-1784 AD Laki (Skaftar Fires) eruption in
746   Iceland. Bull. Vol. 58, 205−225.

747 Tonarini, S., Forte, C., Petrini, R., Ferrara, G., 2003. Melt/biotite $^{11}B/^{10}B$ isotopic fractionation
748   and the boron local environment in the structure of volcanic glasses. Geochim. Cosmochim.
749   Acta 67, 1863− 1873.

750 Tonarini, S., Leeman, W.P., Leat, P.T., 2011. Subduction erosion of forearc mantle wedge
751   implicated in the genesis of the South Sandwich Island (SSI) arc: Evidence from boron
752   isotope systematics. Earth Planet. Sci. Lett. 301, 275−284.

753 Truscott, M.G., Shaw, D.M., Cramer, J.J., 1986. Boron abundance and localization in granulites
754   and the lower continental crust. Bull. Soc. Geol. Finl. 58, 169−177.

755 Turekian, K.K., 1968. *Oceans.* Englewood, Cliffs, NJ, Prentice-Hall, 118 pp.

756 Ulmer, P., Trommsdorff, V., 1995. Serpentine stability to mantle depths and subduction-related
757   magmatism. Science 268, 858−861.

758 Vengosh, A., Starinsky, A., Kolodny, Y., Chivas, A.R., 1991a. Boron isotope geochemistry as a
759   tracer for the evolution of brines and associated hot springs from the Dead Sea, Israel.
760   Geochim. Cosmochim. Acta 55, 1689−1695.

761 Vengosh, A., Chivas, A.R., McCulloch, M.T., Starinsky, A., Kolodny, Y., 1991b. Boron isotope
762   geochemistry of Australian salt lakes. Geochim. Cosmochim. Acta 55, 2591−2606.

763 Walker, R.J., Echeverria, L.M., Shirey, S.B., Horan, M.F., 1991. Re-Os isotopic constraints on
764   the origin of volcanic rocks, Gorgona Island, Colombia: Os isotopic evidence for ancient
765   heterogeneities in the mantle. Contrib. Mineral. Petrol. 107, 150−162.

766 Walker, R.J., Storey, M., Kerr, A.C., Tarney, J., Arndt, N.T., 1999. Implications of ^{187}Os
767   isotopic heterogeneities in a mantle plume: evidence from Gorgona Island and Curaçao.
768   Geochim. Cosmochim. Acta 63, 713−728.

769 Walter, M.J., 1998. Melting of garnet peridotite and the origin of komatiite and depleted
770   lithosphere. J. Petrol. 39, 29−60.

771 Williams, L.B., Hervig, R.L., Holloway, J.R., Hutcheon, I., 2001. Boron isotope geochemistry
772   during diagenesis: Part I. Experimental determination of fractionation during illitization of
773   smectite. Geochim. Cosmochim. Acta 65, 1769– 1782.

774 Wilson, A.H., Shirey, S.B., Carlson, R.W., 2003. Archaean ultra-depleted komatiites formed by
775   hydrous melting of cratonic mantle. Nature 423, 858−861.

776 Wunder, B., Meixner, A., Romer, R.L., Wirth, R., Heinrich, W., 2005. The geochemical cycle of
777   boron: Constraints from boron isotope partitioning experiments between mica and fluid.
778   Lithos 84, 206−216.

779

780

781

Figure captions

Fig. 1. Geological sketch map of Gorgona Island (modified after Echeverría,1980; Kerr et al., 1996; Révillon et al., 2000). Sampling locations are marked by sample numbers referred to in the text.

Fig. 2. Multi-element spectra of the olivine-hosted melt inclusions from Gorgona komatiites, demonstrating positive H_2O, Cl and B enrichment relative to other trace and rare earth elements. Concentrations of trace elements in primitive mantle used for normalization are taken from Hofmann (1998); the normalization values for boron, chlorine and water are 0.3 µg/g B, 17 µg/g Cl and 300 µg/g H_2O, as in Kamenetsky et al. (2010). Shaded field represents the composition of Gorgona picrites, komatiites and D-basalts from Kerr et al. (1996), Arndt et al. (1997), Révillon et al. (2000) and Serrano et al. (2011).

Fig. 3. Boron contents and isotopic composition of the olivine-hosted melt inclusions from Gorgona komatiites. Bars represent ±1 SE analytical precision, shown individually for each B isotope measurement (Y axis) and corresponding to the average ±10% analytical precision in the case of B concentration. The box labeled *Mantle* represents the range of OIB mantle source ($\delta^{11}B = -10 \pm 2‰$ at 0.05–0.25 µg/g B), as suggested by Ryan and Langmuir (1993), Chaussidon and Jambon (1994), Chaussidon and Marty (1995). Dashed arrows visually emphasize two possible trends of magma evolution: (1) the increase of B concentration at nearly constant boron isotopic composition that may be ascribed to high temperature olivine crystallization, and (2) concurrent increase of B concentration and $\delta^{11}B$ values that may result either from magma contamination at shallow depth or from interaction of B-rich subduction-related fluid with mantle source rocks (see discussion).

Fig. 4. Diagrams of (A) Cl/K_2O vs. H_2O/K_2O, (B) B/K_2O vs. H_2O/K_2O, (C) Cl/K_2O vs. B/K_2O and (D) $\delta^{11}B$ vs. B/K_2O (given as weight ratios, except for $\delta^{11}B$ given in ‰) illustrate the effects of addition of different types of contamination products to presumably "uncontaminated" Gorgona komatiitic magma. Mixing lines between presumably "uncontaminated" komatiitic

811   magma (*KOM*) and seawater (*SW*), 15%- and 50%-NaCl saline brines (labeled *15%-NaCl* and

812   *50%-NaCl*, respectively), altered oceanic crust (*AOC*) and siliceous marine sediment (*SED*)

813   calculated from the compositions given in **Table 2** are shown (see text for explanation).

814   Numbers on mixing lines refer to wt% of component added to parent komatiite. Note that mixing

815   lines calculated for 15%- and 50% NaCl brine end-members almost completely overlap between

816   each other in Panel C. The calculated mixing trends allow us to conclude that direct

817   contamination of the Gorgona komatiitic magmas by altered basaltic rocks at shallow depth, as

818   suggested by Arndt et al. (1997), or by seawater or seawater-derived components (saline brine),

819   as discussed in Shimizu et al. (2009), are unable to account for the H_2O, Cl and B enrichment

820   observed in the melt inclusions studied.

821

822   Fig. 5. Diagrams of (A) $\delta^{11}B$ vs. B/Nb and (B) $\delta^{11}B$ vs. Ba/Nb summarize the proposed

823   interpretation of B-isotope variations in olivine-hosted melt inclusions from the Gorgona

824   komatiites. Mixing lines between the depleted MORB-type mantle (MANT), recycled crust

825   (REC), serpentinized peridotite (SERP) and subduction slab fluids (SSF1, SSF2 and SSF3) are

826   shown. Numbers on mixing lines refer to wt% of component added to MANT end-member.
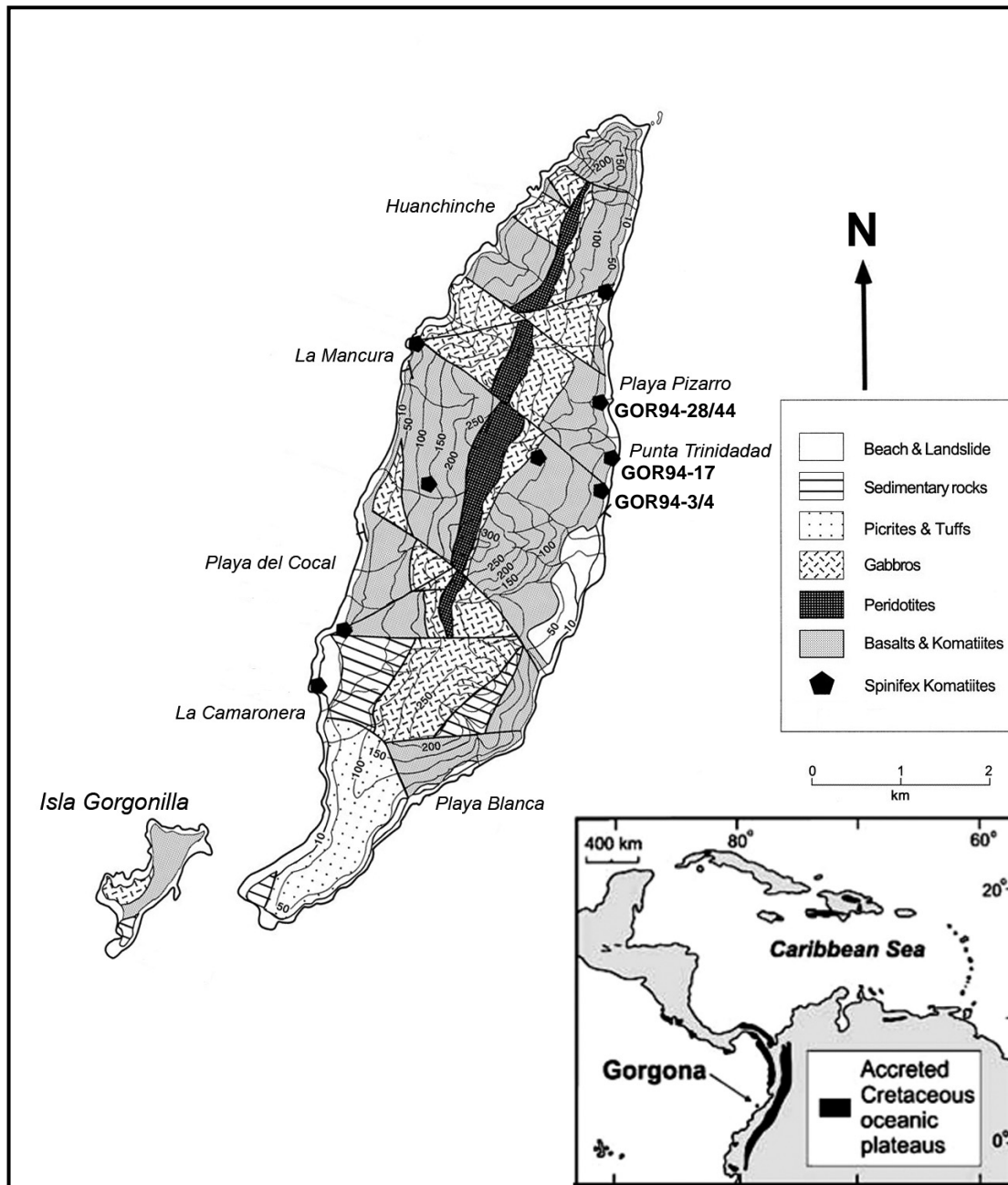
827

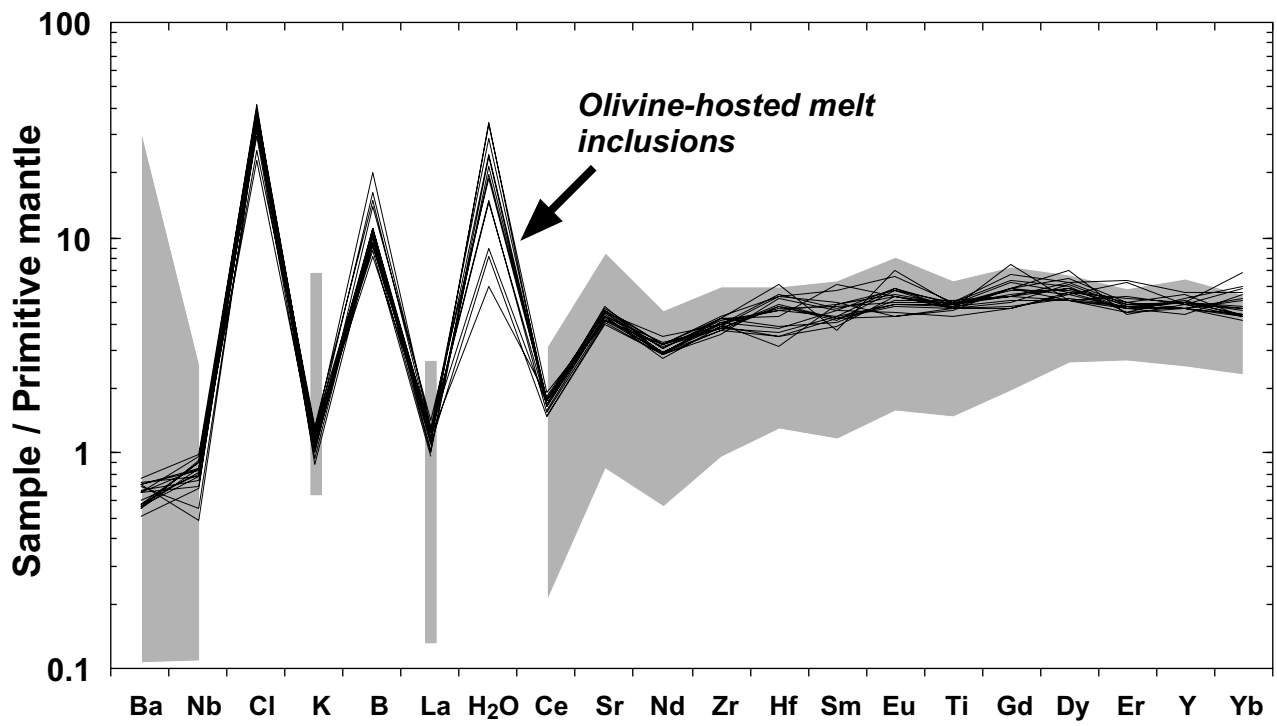Fig. 1. Gurenko and Kamenetsky
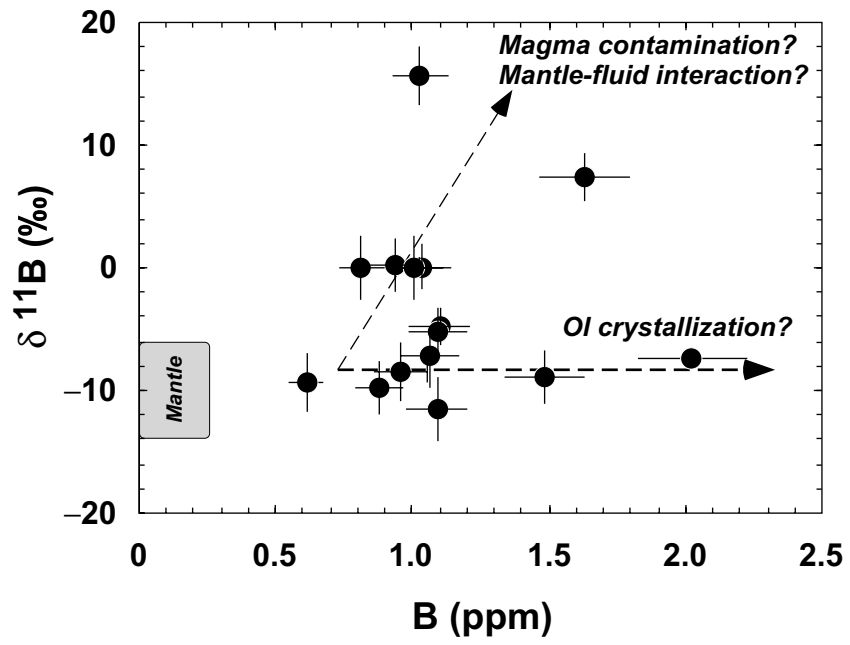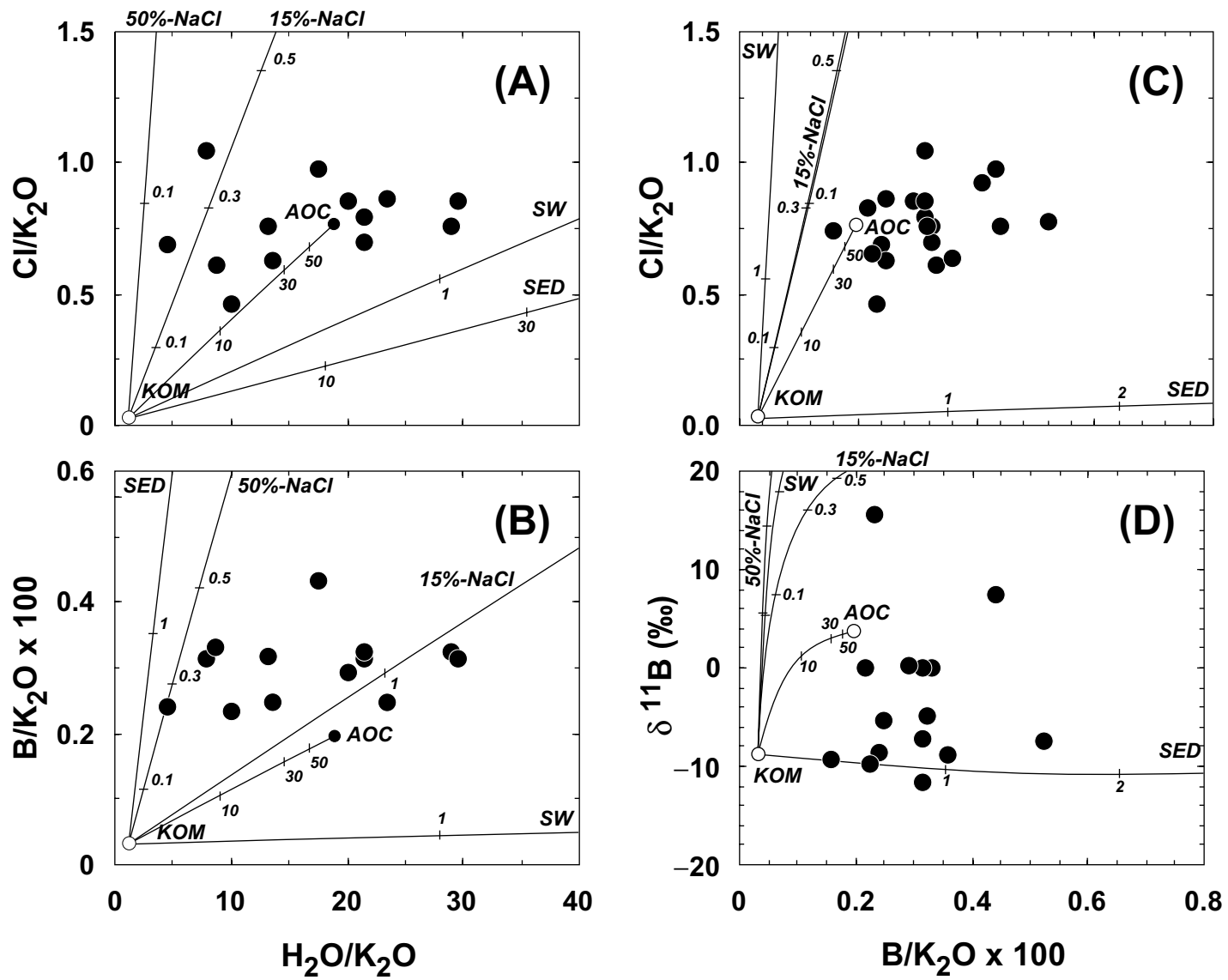
Fig. 2. Gurenko d Kamenetsky

Fig. 3. Gurenko and Kamenetsky
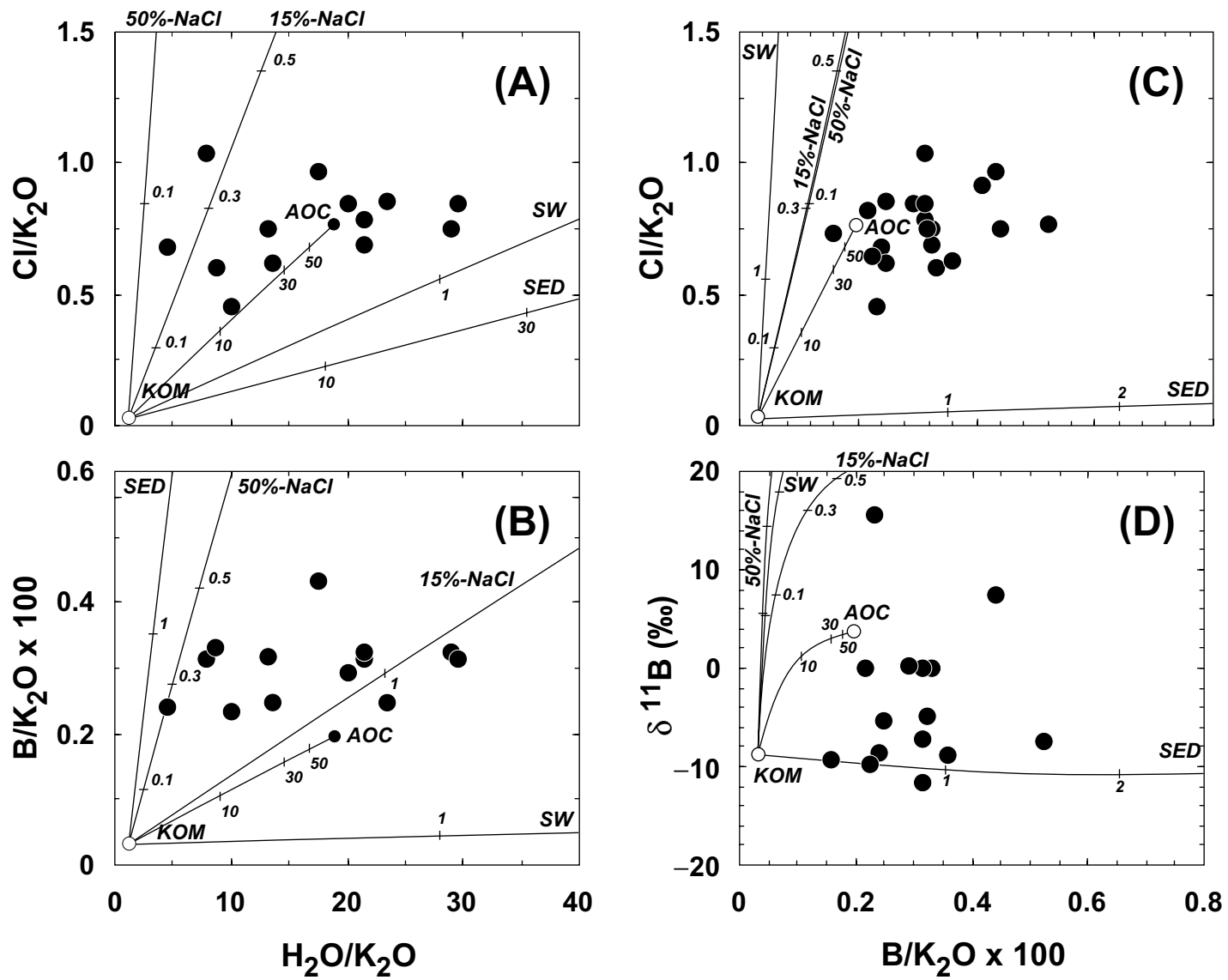
Fig. 4. Gurenko and Kamenetsky
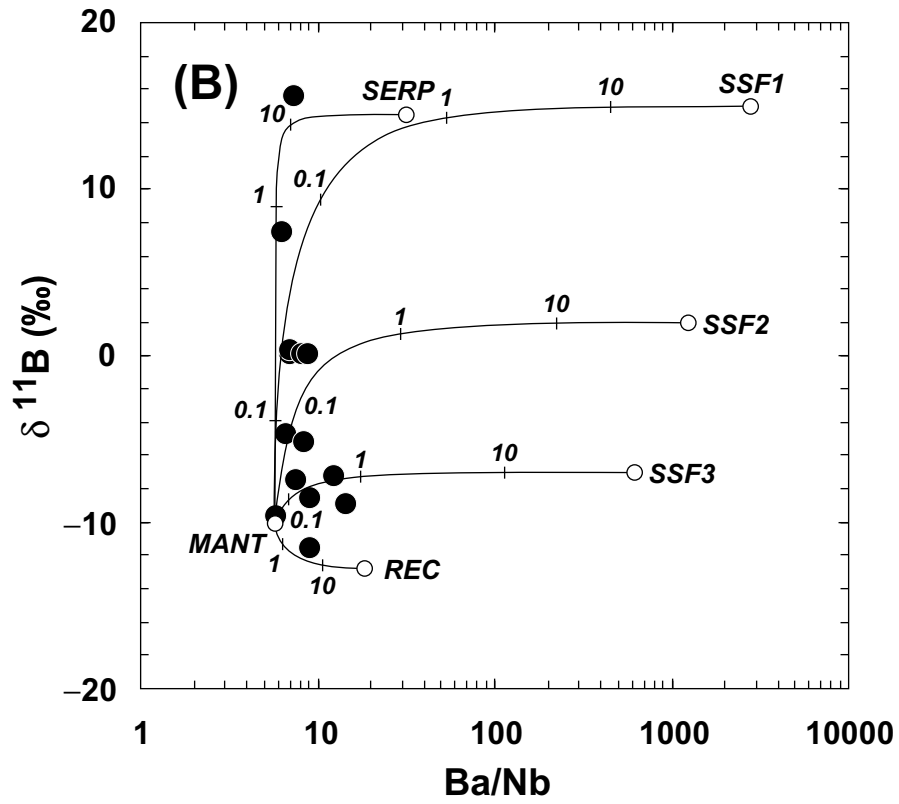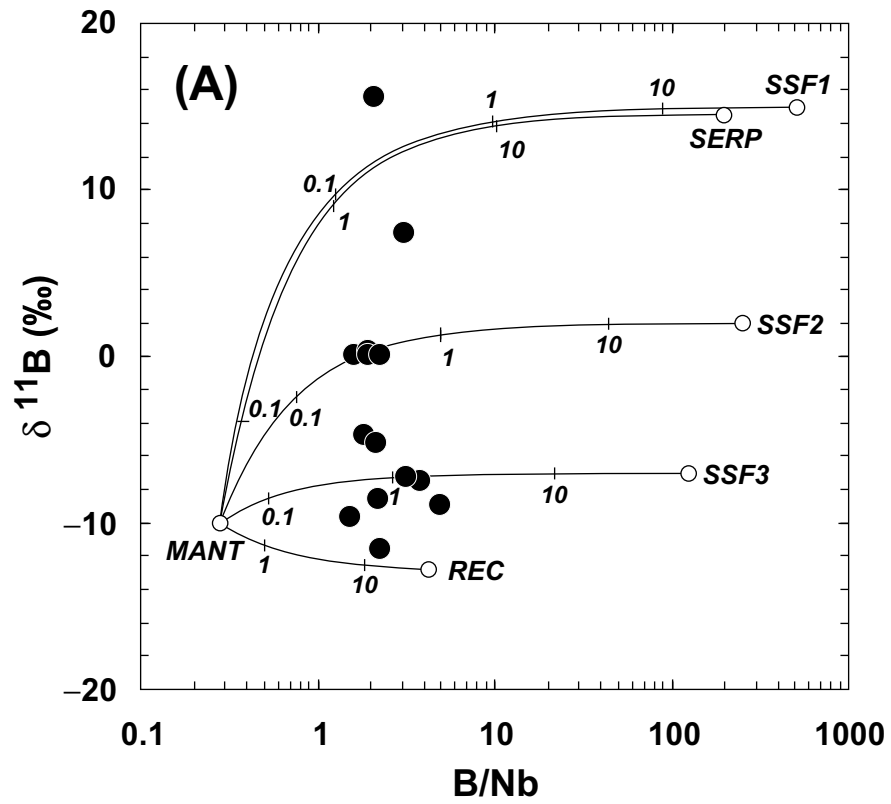
Fig. 4. Gurenko and Kamenetsky

Fig. 5. Gurenke and Kamenetsky

Table 1.

Compositions of the laboratory heated melt inclusions in olivine from Gorgona komatiites, Colombia

Grain No	94-3-30a	94-3-32	94-3-33	94-4-20	94-4-21	94-17-10a	94-17-11	94-17-13	94-17-14	94-17-15	94-17-16	94-28-1	94-28-2	94-28-3a	94-28-7	94-28-8a	94-28-9	94-28-36	94-44-24	94-44-27
Sample	GOR94-3			GOR94-4		GOR94-17						GOR94-28							GOR94-44	
Heated melt inclusions [a]																				
SiO_2	48.25	48.43	48.64	49.02	49.16	48.92	48.61	48.14	48.05	48.59	49.11	49.42	47.98	48.55	48.20	48.84	48.37	47.94	48.94	49.08
TiO2	0.85	0.85	0.83	0.85	0.87	0.85	0.87	0.86	0.88	0.84	0.84	0.95	0.88	0.86	0.88	0.88	0.87	0.86	0.87	0.85
Al_2O_3	15.90	15.85	15.54	15.58	15.91	15.75	15.68	15.60	15.94	15.50	15.46	17.17	16.11	16.12	16.58	16.01	15.79	15.85	15.27	15.50
FeO	6.14	6.91	6.38	6.48	6.23	6.71	6.62	7.11	6.79	7.34	7.57	7.15	7.94	8.37	7.54	8.40	8.90	8.24	6.57	6.56
MnO	0.13	0.13	0.10	0.09	0.09	0.12	0.12	0.15	0.13	0.14	0.15	0.11	0.16	0.18	0.14	0.14	0.13	0.14	0.08	0.11
MgO	11.70	11.45	11.91	11.03	10.76	10.90	10.39	10.76	9.84	10.81	10.95	8.39	9.73	9.92	9.56	9.66	10.06	9.94	10.31	10.43
CaO	13.64	13.75	13.40	13.89	14.17	14.22	14.36	13.88	14.54	13.84	13.79	15.00	14.62	14.07	14.46	14.37	14.13	14.12	14.07	13.95
Na_2O	1.92	1.95	1.89	1.80	1.85	1.83	1.79	1.93	1.92	1.88	1.84	2.12	1.96	1.98	2.06	1.88	1.85	1.89	1.79	1.79
K_2O	0.044	0.030	0.033	0.035	0.044	0.034	0.034	0.034	0.032	0.037	0.032	0.039	0.037	0.039	0.033	0.038	0.040	0.032	0.041	0.039
P_2O_5	0.046	0.054	0.055	0.058	0.061	0.062	0.044	0.052	0.047	0.052	0.054	0.070	0.061	0.062	0.067	0.057	0.056	0.065	0.051	0.046
S	0.052	0.068	0.066	0.056	0.056	0.058	0.052	0.056	0.071	0.063	0.064	0.071	0.077	0.073	0.071	0.072	0.076	0.076	0.052	0.059
Cl	0.023	0.025	0.023	0.029	0.025	0.025	0.026	0.025	0.025	0.022	0.022	0.029	0.028	0.030	0.031	0.031	0.029	0.027	0.026	0.026
Total	98.69	99.49	98.87	98.92	99.22	99.39	98.62	98.60	98.17	99.03	99.88	100.52	99.58	100.24	99.51	100.39	100.31	99.09	98.08	98.44
Host olivine																				
SiO_2	40.84	41.02	40.38	40.34	40.28	40.68	40.80	40.74	40.69	40.32	40.42	40.35	41.34	40.66	41.24	40.22	40.40	40.64	40.68	40.69
FeO	8.48	9.18	8.61	9.37	9.03	9.61	9.72	9.54	9.81	10.39	10.08	9.21	9.02	8.90	8.85	8.97	8.95	9.25	8.65	8.88
MnO	0.12	0.15	0.14	0.14	0.16	0.15	0.17	0.13	0.15	0.16	0.17	0.15	0.15	0.15	0.15	0.14	0.14	0.15	0.12	0.14
MgO	49.99	49.71	49.26	48.81	48.88	48.86	49.06	49.19	48.86	48.05	48.36	49.01	50.02	49.48	50.17	48.56	48.91	49.32	49.45	49.44
CaO	0.31	0.34	0.32	0.32	0.32	0.32	0.33	0.33	0.33	0.34	0.34	0.32	0.33	0.32	0.32	0.32	0.32	0.31	0.32	0.31
NiO	0.44	0.45	0.43	0.42	0.44	0.42	0.40	0.41	0.42	0.39	0.40	0.43	0.44	0.44	0.45	0.44	0.43	0.42	0.44	0.44
Cr_2O_3	0.12	0.13	0.12	0.12	0.11	0.11	0.10	0.12	0.10	0.09	0.11	0.11	0.13	0.12	0.12	0.14	0.14	0.10	0.12	0.11
Total	100.31	100.98	99.25	99.52	99.21	100.14	100.57	100.46	100.36	99.74	99.87	99.56	101.43	100.07	101.30	98.79	99.29	100.19	99.78	100.00
Fo	91.3	90.6	91.1	90.3	90.6	90.1	90.0	90.2	89.9	89.2	89.5	90.5	90.8	90.8	91.0	90.6	90.7	90.5	91.1	90.9
Compositions and temperatures of the trapped melts (normalized to 100%) [b]																				
SiO_2	46.4	46.7	46.8	47.3	47.0	47.1	47.1	46.9	46.8	47.4	47.4	46.7	46.2	46.5	46.2	46.7	46.6	46.6	47.2	47.2
TiO_2	0.7	0.7	0.7	0.7	0.7	0.7	0.7	0.7	0.7	0.7	0.7	0.7	0.7	0.7	0.7	0.7	0.7	0.7	0.7	0.7
Al_2O_3	12.7	13.2	12.6	12.9	12.8	13.1	13.1	13.2	13.4	13.6	13.3	13.2	13.0	13.0	13.1	12.9	13.0	13.2	12.1	12.4
Fe_2O_3	1.4	1.4	1.4	1.4	1.4	1.38	1.4	1.4	1.4	1.4	1.4	1.4	1.4	1.4	1.4	1.4	1.4	1.4	1.4	1.4
FeO	9.6	9.6	9.6	9.6	9.6	9.56	9.6	9.6	9.6	9.6	9.6	9.6	9.6	9.6	9.6	9.6	9.6	9.6	9.6	9.6
MnO	0.1	0.1	0.1	0.1	0.1	0.1	0.1	0.1	0.1	0.1	0.1	0.1	0.2	0.2	0.1	0.1	0.1	0.1	0.1	0.1
MgO	16.6	15.3	16.3	14.9	15.4	14.5	14.4	14.6	14.1	13.3	13.8	15.0	15.4	15.6	15.8	15.3	15.4	15.0	16.3	15.9
CaO	10.9	11.4	10.9	11.6	11.4	11.9	12.0	11.8	12.2	12.2	11.9	11.6	11.8	11.4	11.4	11.6	11.7	11.8	11.2	11.2
Na_2O	1.5	1.6	1.5	1.5	1.5	1.5	1.5	1.6	1.6	1.7	1.6	1.6	1.6	1.6	1.6	1.5	1.5	1.6	1.4	1.4
K_2O	0.03	0.03	0.02	0.03	0.03	0.03	0.03	0.03	0.03	0.04	0.03	0.03	0.03	0.03	0.02	0.03	0.03	0.03	0.03	0.03
P_2O_5	0.04	0.04	0.04	0.05	0.05	0.05	0.03	0.04	0.04	0.04	0.04	0.05	0.05	0.05	0.06	0.05	0.05	0.05	0.04	0.04
T_{calc} ºC	1383	1358	1376	1347	1358	1339	1337	1343	1332	1314	1325	1352	1362	1365	1370	1357	1359	1352	1375	1368
Ol-add	24.0	18.9	21.7	19.4	22.7	18.2	19.1	17.7	19.2	13.0	14.2	27.1	22.8	22.4	25.5	21.9	20.0	19.9	26.2	24.7

Table 1 (*Continued*)

Grain No	94-3-30a	94-3-32	94-3-33	94-4-20	94-4-21	94-17-10a	94-17-11	94-17-13	94-17-14	94-17-15	94-17-16	94-28-1	94-28-2	94-28-3a	94-28-7	94-28-8a	94-28-9	94-28-36	94-44-24	94-44-27
Sample	GOR94-3			GOR94-4		GOR94-17						GOR94-28							GOR94-44	

Boron isotopes, volatiles and trace elements [c]

	94-3-30a	94-3-32	94-3-33	94-4-20	94-4-21	94-17-10a	94-17-11	94-17-13	94-17-14	94-17-15	94-17-16	94-28-1	94-28-2	94-28-3a	94-28-7	94-28-8a	94-28-9	94-28-36	94-44-24	94-44-27
$\delta^{11}B$, ‰	15.6	0.1	0.1	−11.5	−5.3	ND	−4.8	−7.3	ND	ND	0.3	−9.3	7.4	−7.5	ND	0.0	−8.5	ND	−8.9	−9.7
1σ SE	2.4	2.6	1.8	2.7	2.0	ND	1.5	2.6	ND	ND	2.2	2.5	2.0	1.9	ND	2.6	2.3	ND	2.2	2.2
H_2O	0.44	0.27	0.71	1.03	0.59	1.00	0.73	0.44	0.57	0.87	0.64	ND	ND	ND	ND	ND	0.18	0.25	ND	ND
Cl	205	184	262	296	277	260	236	254	315	321	273	285	280	300	305	313	272	330	263	257
B	1.03	1.01	1.04	1.09	1.10	1.1	1.10	1.07	1.4	0.9	0.93	0.61	1.63	2.02	1.4	0.81	0.95	1.0	1.48	0.88
K	334	270	284	299	308	275	246	265	262	313	290	ND	307	321	274	313	288	228	343	327
Ti	5081	5369	5129	5357	5266	5383	5120	5198	5215	5599	5097	ND	5413	5333	5333	5313	5395	4713	5022	5130
V	405	406	406	453	412	484	369	388	378	462	397	ND	ND	ND	ND	ND	435	300	ND	ND
Cr	686	706	825	736	579	ND	751	444	741	716	484	ND	ND	ND	ND	ND	401	778	ND	ND
Sr	77.0	79.2	78.5	82.2	80.2	75.8	75.2	75.0	81.3	84.3	75.0	ND	86.4	83.3	84.9	86.8	82.3	72.7	78.1	73.7
Y	19.8	19.6	18.7	18.6	19.6	20.7	18.4	18.7	20.4	19.5	19.4	ND	22.0	19.9	22.0	21.5	19.4	17.4	19.5	18.3
Zr	37.9	39.1	38.0	38.2	39.2	38.5	36.5	37.0	38.8	41.0	35.7	ND	42.3	40.9	42.0	41.3	40.4	34.2	37.1	35.9
Nb	0.49	0.52	0.46	0.48	0.51	0.56	0.60	0.34	0.42	0.61	0.48	ND	0.53	0.53	0.42	0.50	0.44	0.56	0.30	0.57
Ba	3.67	4.31	4.06	4.46	4.29	3.52	3.98	4.27	3.07	4.65	3.42	ND	3.35	4.00	4.07	3.49	3.94	3.40	4.36	3.37
La	0.77	0.77	0.63	0.69	0.71	0.71	0.77	0.77	0.87	0.80	0.61	ND	0.81	0.79	0.46	0.77	0.73	0.68	0.77	0.59
Ce	2.71	2.70	2.63	2.65	2.87	3.09	2.81	2.47	2.83	2.83	2.80	ND	2.82	2.72	2.35	2.70	2.94	2.35	2.54	2.38
Pr	0.59	0.55	0.51	0.64	0.56	0.69	0.57	0.60	0.64	0.53	0.55	ND	0.67	0.50	0.66	0.51	0.70	0.44	0.52	0.33
Nd	3.52	3.40	3.26	3.46	3.46	3.81	3.84	3.72	4.17	3.80	3.50	ND	3.81	3.61	3.12	3.43	3.61	3.42	3.89	3.45
Sm	1.92	1.68	1.51	1.89	1.80	1.84	1.68	1.62	1.83	1.57	1.64	ND	2.18	1.44	1.79	2.34	1.88	1.77	1.62	1.60
Eu	0.63	0.71	0.77	0.80	0.85	0.73	0.84	0.72	0.77	0.75	0.69	ND	0.96	1.03	0.60	0.78	0.83	0.65	0.62	0.82
Gd	2.46	3.15	2.96	2.74	2.77	3.23	2.55	2.61	2.97	2.74	2.41	ND	3.44	2.93	2.41	2.98	2.76	2.43	2.95	3.85
Tb	0.51	0.59	0.58	0.51	0.56	0.55	0.52	0.51	0.51	0.57	0.56	ND	0.64	0.59	0.51	0.54	0.56	0.54	0.49	0.54
Dy	3.33	3.52	3.29	3.67	3.71	3.81	3.89	3.28	3.46	3.95	3.47	ND	3.96	3.64	3.57	4.09	3.29	3.55	4.47	3.30
Ho	0.67	0.66	0.71	0.74	0.74	0.84	0.62	0.63	0.59	0.71	0.75	ND	0.81	0.75	0.84	0.91	0.78	0.69	0.65	0.53
Er	2.00	2.16	1.94	2.08	1.98	1.86	2.01	1.89	1.97	2.05	2.61	ND	2.64	2.05	2.00	2.09	2.20	1.94	1.85	2.00
Tm	0.25	0.24	0.29	0.30	0.25	0.27	0.25	0.30	0.27	0.25	0.33	ND	0.34	0.29	0.25	0.32	0.29	0.24	0.38	0.28
Yb	1.83	1.98	2.15	1.83	1.92	2.49	2.10	1.72	1.80	1.96	2.40	ND	2.29	2.88	2.76	1.80	1.94	2.24	1.79	1.79
Lu	0.26	0.28	0.32	0.31	0.35	0.30	0.26	0.23	0.27	0.32	0.32	ND	0.31	0.28	0.24	0.30	0.30	0.30	0.22	0.28
Hf	1.43	1.22	0.94	0.84	1.02	1.25	0.98	1.28	1.46	1.03	0.93	ND	1.44	1.63	1.53	1.16	1.24	1.40	1.31	1.27
Pb	0.40	0.16	0.06	0.11	ND	0.30	ND	0.59	0.71	0.37	0.36	ND	0.10	0.20	0.30	0.09	0.12	0.38	ND	0.05
Th	ND	0.02	0.02	0.02	0.01	0.06	0.02	0.04	0.03	0.03	ND	ND	0.03	0.03	ND	0.02	0.03	0.02	ND	0.02
B/K	0.0031	0.0037	0.0037	0.0036	0.0036	0.0040	0.0045	0.0040	0.0053	0.0029	0.0032	0.0019	0.0053	0.0063	0.0049	0.0026	0.0033	0.0043	0.0043	0.0027
$[La/Sm]_n$	0.25	0.29	0.26	0.23	0.25	0.24	0.29	0.30	0.30	0.32	0.24	–	0.23	0.35	0.16	0.21	0.24	0.24	0.30	0.23
$[H_2O/Nb]_n$	19	10	32	44	24	37	25	27	28	29	28	–	–	–	–	–	8	9	–	–
$[Cl/Nb]_n$	32	27	44	47	42	36	31	58	57	41	44	–	41	44	56	48	48	46	68	35
$[B/Nb]_n$	13	12	14	14	13	12	11	19	20	9	12	–	19	24	20	10	14	11	30	10

2

Notes for Table 1.

[a] Major element concentrations of the laboratory heated melt inclusions and their host olivines (given in wt%) were analyzed using the JEOL JXA-8200 electron microprobe at the Max Planck Institute for Chemistry (Mainz, Germany) at standard conditions (Kamenetsky et al., 2010). A set of reference materials (i.e. natural and synthetic oxides, minerals and glasses; Micro-Analysis Consultants Ltd, Cambridgeshire, UK) and the Smithsonian Institution standard set for electron microprobe analysis (Jarosewich et al., 1980) were used for routine calibration and instrument stability monitoring. Typical analytical uncertainties (2RSD = 2σ relative standard deviation) are 1.5−3.0% for SiO_2, Al_2O_3, FeO, MgO, CaO, TiO_2; 4−6% for Na_2O, 10% for K_2O, 15% for P_2O_5, and 30% for MnO. As a monitor sample for S and Cl measurements, we also used the USNM 111240/52 VG-2 basaltic glass (recommended values of 0.134−0.137 wt.% S; 0.030 wt.% Cl; Dixon et al., 1991; Thordarson et al., 1996; N. Metrich, personal communication, 2003). The concentrations of 0.140 ± 0.023 wt.% S and 0.029 ± 0.007 wt.% Cl (±2σ SD = 2-sigma standard deviation, N = 37) were obtained during this study (for more detail see Kamenetsky et al., 2010). Fo = mol% of forsterite component of the host olivine.

[b] Calculated compositions and temperatures of the trapped komatiitic melts are based on the compositions of the laboratory heated melt inclusions, corrected for "Fe-loss" and post-entrapment crystallization of host mineral (for detail see Kamenetsky et al., 2010); Ol-add = total amount of olivine (wt%) "added" to the included melts during correction.

[c] Boron isotope composition (in permil units) calculated relative to the NBS 951 standard ($^{11}B/^{10}B$ = 4.04558 ± 0.00033; Spivack and Edmond, 1986) given at ±1σ SE analytical precision (see text for detail). The contents of volatile components (H_2O given in wt%, Cl in µg/g) and trace element concentrations (given in µg/g) were analyzed using the CAMECA IMS 3f ion microprobe and the single collector sector-field ICP-MS Element 2 instrument equipped with the New Wave Research UP213 Nd-YAG (213 nm) laser, both located in the Max Planck Institute for Chemistry, Mainz, Germany (raw values uncorrected for post-entrapment olivine crystallization in melt inclusions are given; for more detail see Kamenetsky et al., 2010). The $[La/Sm]_n$, $[H_2O/Nb]_n$, $[Cl/Nb]_n$ and $[B/Nb]_n$ are element ratios normalized to primitive mantle (PM; assuming 300 µg/g H_2O, 8 µg/g Cl and 0.1 µg/g B, while Nb concentration of 0.6175 µg/g is taken from Hofmann, 1988). ND = not determined, − = no value.

Table 2.
Compositions of the end-members used for calculation of mixing lines (see text for more details).

Component	B	$\delta^{11}B$	H_2O	Cl	K	Ba	Nb
Unit	µg/g	‰	wt%	µg/g	µg/g	µg/g	µg/g
KOM[a]	0.118	−9.0	0.042	7.38	309	4.1	0.44
SW[b]	4.5	+39.5	97.5	19350	392	0.021	1.50E-05
15%-NaCl[c]	100	+25.5	85	99000	2076	0.111	7.94E-05
50%-NaCl[c]	312	+56.6	50	303000	6476	0.347	2.48E-04
AOC[d]	5.2	+3.7	5	2040	2200	22.6	1.22
REC[e]	5.2	−12.8	–	–	–	22.6	1.22
SED[f]	120	−10.0	8.2	1000	1245	1950	2.44
MANT[g]	0.06	−10.0	116	0.51	60	1.2	0.21
SERP[h]	20	+14.5	–	–	–	3.2	0.1
SSF1[i]	200	+15.0	–	–	–	1000	0.36
SSF2[i]	100	+2.0	–	–	–	500	0.36
SSF3[i]	50	−7	–	–	–	250	0.36

[a] KOM = "uncontaminated" komatiitic magma representing average composition of seven, the most ^{11}B-depleted melt inclusions (i.e., 94-28-1, -28-3mi1, -28-9, -4-20, -44-27, -17-13, -44-24; Table 1). The concentrations of H_2O, Cl and B were calculated from the concentrations of neighboring elements of similar incompatibility: $[H_2O]_n = ([La]_n \times [Ce]_n)^{0.5}$, $[Cl]_n = ([Nb]_n \times [K]_n)^{0.5}$ and $[B]_n = ([K]_n \times [La]_n)^{0.5}$.

[b] SW = seawater composition at 3.5% salinity.

[c] 15%- and 50%-NaCl brines.

[d] AOC = altered oceanic crust.

[e] REC = recycled crust.

[f] SED = siliceous marine sediment.

[g] MANT = mantle component of the Gorgona komatiite magma source.

[h] SERP = recycled forearc serpentinite.

[i] SSF1-SSF3 = subducting slab fluids.